Borexino calibrations: hardware, methods, and results

2012 JINST 7 P10018

(http://iopscience.iop.org/1748-0221/7/10/P10018)

Jinst

PUBLISHED BY IOP PUBLISHING FOR SISSA MEDIALAB

RECEIVED: *July 24, 2012*
ACCEPTED: *September 27, 2012*
PUBLISHED: *October 22, 2012*

Borexino calibrations: hardware, methods, and results

Borexino Collaboration

H. Back,[3] G. Bellini,[1] J. Benziger,[6] D. Bick,[17] G. Bonfini,[2] D. Bravo,[3] M. Buizza Avanzini,[5] B. Caccianiga,[1,*] L. Cadonati,[16] F. Calaprice,[4] C. Carraro,[7] P. Cavalcante,[2] A. Chavarria,[4] A. Chepurnov,[18] D. D'Angelo,[1] S. Davini,[7,20] A. Derbin,[9] A. Etenko,[10] F. von Feilitzsch,[8] G. Fernandes,[7] K. Fomenko,[11] D. Franco,[5] C. Galbiati,[4] S. Gazzana,[2] C. Ghiano,[2] M. Giammarchi,[1] M. Goeger-Neff,[8] A. Goretti,[4] L. Grandi,[4] E. Guardincerri,[7] S. Hardy,[3] Aldo Ianni,[2] Andrea Ianni,[4] A. Kayunov,[9] S. Kidner,[3] V. Kobychev,[19] D. Korablev,[11] G. Korga,[13,20] Y. Koshio,[2] D. Kryn,[5] M. Laubenstein,[2] T. Lewke,[8] E. Litvinovich,[10] B. Loer,[4] F. Lombardi,[2] P. Lombardi,[1] L. Ludhova,[1] I. Machulin,[10] S. Manecki,[3] W. Maneschg,[12] G. Manuzio,[7] Q. Meindl,[8] E. Meroni,[1] L. Miramonti,[1] M. Misiaszek,[14] D. Montanari,[2,4] P. Mosteiro,[4] V. Muratova,[9] L. Oberauer,[8] M. Obolensky,[5] F. Ortica,[15] K. Otis,[16] M. Pallavicini,[7] L. Papp,[13,3] L. Perasso,[7] S. Perasso,[7] A. Pocar,[16] R.S. Raghavan,[3] G. Ranucci,[1] A. Razeto,[2] A. Re,[1] A. Romani,[15] N. Rossi,[2] D. Rountree,[3] A. Sabelnikov,[10] R. Saldanha,[4] C. Salvo,[7] S. Schönert,[8] H. Simgen,[12] M. Skorokhvatov,[10] O. Smirnov,[11] A. Sotnikov,[11] S. Sukhotin,[10] Y. Suvorov,[10,21] R. Tartaglia,[2] G. Testera,[7] D. Vignaud,[5] R.B. Vogelaar,[3] J. Winter,[8] M. Wojcik,[14] A. Wright,[4] M. Wurm,[17] J. Xu,[4] O. Zaimidoroga,[11] S. Zavatarelli[7] and G. Zuzel[14]

[1] *Dipartimento di Fisica, Università di Milano and INFN Milano, via Celoria 16, I-20133 Milano, Italy*

[2] *Laboratori Nazionali del Gran Sasso, SS 17bis Km 18+910, I-67010 Assergi (AQ), Italy*

[3] *Physics Department, Robeson Hall, Virginia Polytechnic Institute and State University, Blacksburg, VA 24061-0435, U.S.A.*

[4] *Department of Physics, Princeton University, Jadwin Hall, Washington Road, Princeton, NJ 08544-0708, U.S.A.*

[5] *Astroparticule et Cosmologie APC, 10 rue Alice Domon et Léonie Duquet, 75205 Paris cedex 13, France*

[6] *Department of Chemical Engineering, Princeton University, Engineering Quadrangle, Princeton, NJ 08544-5263, U.S.A.*

[*] Corresponding author.

doi:10.1088/1748-0221/7/10/P10018

2012 JINST 7 P10018

[7] *Dipartimento di Fisica, Università di Genova and INFN Genova, via Dodecaneso 33, I-16146 Genova, Italy*
[8] *Technische Universität München, James Franck Strasse E15, D-85747 Garching, Germany*
[9] *St. Petersburg Nuclear Physics Institute, Gatchina, Russia*
[10] *NRC Kurchatov Institute, Kurchatov Sq. 1, 123182 Moscow, Russia*
[11] *JINR, Joliot Curie str. 6, 141980 Dubna, Russia*
[12] *Max-Planck-Institut für Kernphysik, Saupfercheckweg 1, D-69117 Heidelberg, Germany*
[13] *KFKI-RMKI, 1121 Budapest, Hungary*
[14] *Institute of Physics, Jagiellonian University, ul. Reymonta 4, PL-30059 Krakow, Poland*
[15] *Dipartimento di Chimica, Università di Perugia and INFN Perugia, via Elce di Sotto 8, I-06123 Perugia, Italy*
[16] *Physics Department, University of Massachusetts, Amherst, MA 01003, U.S.A.*
[17] *Institut für Experimentalphysik, Universität Hamburg, 22761 Hamburg, Germany*
[18] *Physics Department, Lomonosov Moscow State University, 119899, Moscow, Russia*
[19] *Institute for Nuclear Research, 03680 Kiev, Ukraine*
[20] *Physics Department, University of Houston, Houston, TX 77204, U.S.A.*
[21] *Physics and Astronomy Department, University of California Los Angeles, Los Angeles, CA 90095, U.S.A.*

E-mail: spokeperson@borex.lngs.infn.it

ABSTRACT: Borexino was the first experiment to detect solar neutrinos in real-time in the sub-MeV region. In order to achieve high precision in the determination of neutrino rates, the detector design includes an internal and an external calibration system. This paper describes both calibration systems and the calibration campaigns that were carried out in the period between 2008 and 2011. We discuss some of the results and show that the calibration procedures preserved the radiopurity of the scintillator. The calibrations provided a detailed understanding of the detector response and led to a significant reduction of the systematic uncertainties in the Borexino measurements.

KEYWORDS: Calorimeters; Large detector systems for particle and astroparticle physics

ARXIV EPRINT: 1207.4816

2012 JINST 7 P10018

Contents

2012 JINST 7 P10018

1 Introduction

Borexino is a large volume liquid scintillator detector located at the Laboratori Nazionali del Gran Sasso (LNGS), Italy. The main goal of this experiment is the study of the low energy part of the solar neutrino spectrum in the sub-MeV region, in particular the monochromatic ^{7}Be neutrinos. Borexino succeeded to perform the first real-time detection of ^{7}Be neutrinos [1] and measured the ^{7}Be neutrino flux and its day/night asymmetry [2–4] with a high precision. Furthermore, a detailed solar neutrino spectroscopic measurement of the solar *pep* and ^{8}B neutrinos was carried out and the most most stringent limit on the CNO neutrino rate was determined [5, 6]. Borexino also proved to be a clean anti-neutrino detector that was able to observe geo-neutrinos [7] and to set new limits on anti-neutrino fluxes from the Sun and other unknown sources [8]. Finally, the extremely clean environment of the Borexino detector allowed to search for rare or even forbidden processes like Pauli violating transitions [9], or for axions produced in the Sun [10].

The key requirements for the success of Borexino are the radiopurity of its scintillator and the complete knowledge of the detector's response. The latter is needed for several reasons: since the neutrino interaction rate is determined from a fit to the scattered electron energy spectrum, it is necessary to determine the energy scale to high precision over a broad energy range (between 0.1 and 10 MeV depending on the analysis). The large dimensions of the detector require a careful mapping of its energy response in different positions within the scintillating volume. Another important issue is the testing and tuning of α/β discrimination techniques. Finally, most analyses rely on the offline software-cut selection of scintillator subvolumes (so-called fiducial volumes (FV)) that optimize the signal-to-background ratio. Thus, it is critical as well to validate the position reconstruction algorithm, as this reduces systematic uncertainties in the evaluation of the target mass. All tasks can be accomplished through calibrations using sources of different types (α, β, γ and neutron emitters; laser source) that cover different energy regions.

During the first period of data-acquisition from May 2007 until October 2008, no radioactive sources were inserted into the detector due to the risk of contamination of the highly radiopure scintillator. At that time, contaminants already present in the detector such as ^{14}C and ^{222}Rn or the cosmogenically produced ^{11}C were used as calibration candles allowing the first measurement of the ^{7}Be neutrino rate with a total uncertainty budget of $\simeq$ 10% [1, 2]. To improve this result, several calibration campaigns were performed starting from October 2008. Sources of different types were deployed in different positions within the detector. The calibrations provided a detailed understanding of the detector response, which, in case of the ^{7}Be neutrino rate made possible to reduce the systematic uncertainty from 8.5% to less than 2% [3, 4].

This paper is devoted to the description of the Borexino calibration systems and calibration campaigns. Two separate sub-systems are presented. The first one is the internal calibration system which was designed for the insertion of radioactive sources at different positions within the scintillator volume. The second one is the external calibration system that was used to deploy γ sources into the buffer region around the stainless steel sphere. Both systems were carefully designed to comply with the stringent radiopurity specifications of the Borexino experiment.

Section 2 briefly describes the Borexino detector. Section 3 is devoted to the internal calibration system: hardware, sources and calibration procedures are described. Similarly, section 4 is devoted to the description of the external calibration system. Several relevant examples of results ob-

2012 JINST 7 P10018

tained from the calibrations are presented in section 5. These results show that the calibration systems worked properly and that the calibrations significantly improved Borexino's physics results.

2 The Borexino detector

Borexino is located deep underground at 3,800 meters of water equivalent, in the Hall C of the Laboratori Nazionali del Gran Sasso (LNGS). At this depth the cosmic muon flux is reduced by a factor $\sim 10^6$. Borexino detects neutrinos through the elastic scattering interaction with electrons in the organic liquid scintillator. Anti-neutrinos are detected via the inverse neutron beta-decay. The detector design follows the concept of graded shielding, in which concentric material layers of increasing radiopurity shield the innermost ultra-pure core of the experiment. A schematic view of the Borexino structure is depicted in figure 1. The detection medium is an organic liquid scintillator consisting of 278 tons (315 m^3) of pseudocumene (1,2,4-trimethylbenzene) as a solvent doped with 1.5 g/l PPO (2,5-diphenyloxazole) as a solute. The scintillator needs to be exceptionally radiopure to be capable of detecting the feeble neutrino signal (which amounts to a few tens of counts/(day$\times$100 ton). A dedicated purification strategy including distillation and sparging with ultrapure nitrogen has been developed during 15 years of R&D studies and was successful in reducing background down to the required levels. As an example, the residual ^{238}U and ^{232}Th concentrations in the scintillator are $(1.6\pm0.1)\times10^{-17}$g/g and $(6.8\pm1.5)\times10^{-18}$g/g, respectively: these unprecedented levels of radiopurity even exceed the design goals. The scintillator is contained in a spherical nylon balloon of radius R=4.25 m. This inner vessel (IV) is viewed by 2214 photomultiplier tubes (PMTs) mounted on a concentric stainless steel sphere (SSS) of radius R=6.85 m. Between the SSS and the IV an ultra-pure buffer liquid (pseudocumene + DMP to quench scintillation light) effectively minimizes the diffusion of radioactive particles and the penetration of external radiation from the PMTs, 1843 light concentrators (LCs), and the SSS. A spherical nylon barrier (Outer Vessel, OV) concentric with the IV prevents Radon emanated from the materials on the SSS to reach the scintillating core of the detector. Further shielding against radioactivity from the surrounding rocks is provided by 2100 tons of ultra-pure water in a domed steel tank 16.9 m in height and 18 m in diameter. This outer detector (OD) embeds the SSS containing the inner detector (ID). The OD is also equipped with PMTs to detect Cherenkov light emitted by residual cosmic muons crossing the water. More details about the Borexino detector and about its purification facilities are presented in [11, 12].

In this context, calibrations are an important and delicate issue: in fact, the necessity to preserve the detector radiopurity poses severe constraints on the system design and raises several problems from the operational point of view. We show in this paper that these difficulties have been overcome and that the system has worked properly, becoming an important element for the success of the Borexino experiment.

3 Internal source calibration

3.1 Hardware

The internal calibration system of the Borexino detector has a complex structure that consists of two sub-systems. The first one is the calibration source deployment system (section 3.1.1) used to deploy radioactive or laser sources into the desired location within the scintillator. The hardware

2012 JINST 7 P10018

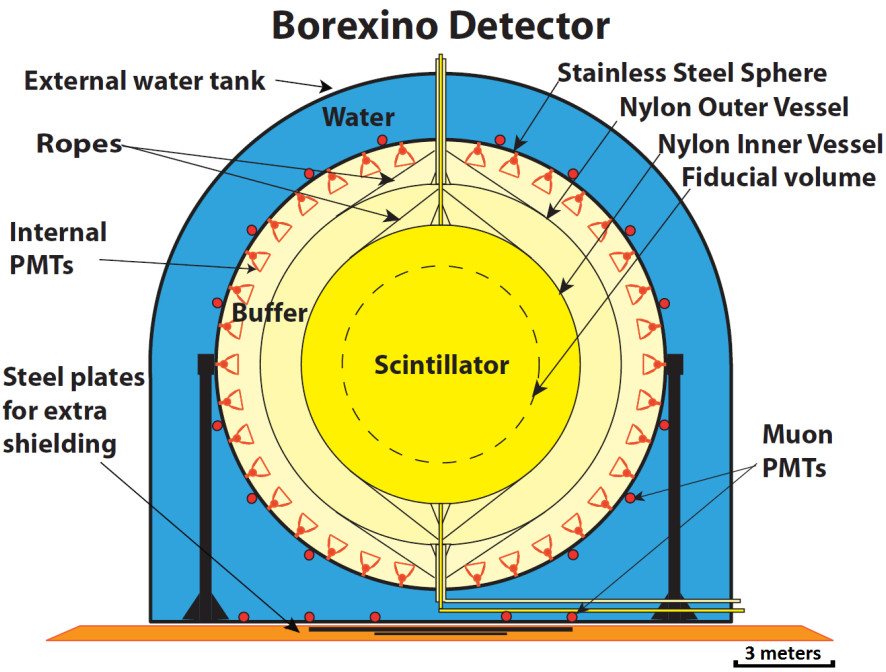

Figure 1. Schematic view of the Borexino detector.

design incorporates solutions to several obstacles related to the detector requirements and provides operational comfort during calibration campaigns. For instance, even though all the operations can be performed by only one operator, the hardware design allows for two people to share the same task. The second sub-system is the source location system (section 3.1.2) used to determine the source reference position with a precision of better than 1 cm.

3.1.1 Source insertion system

Due to the detector's specific design the only access to the scintillator volume is through a 4" diameter pipe connecting the IV to a gate valve on top of the water tank — a vertical distance of six meters (see figure 2). The source deployment system itself is made up of a series of interconnecting hollow rods, assembled into an arm that can be bent up to 90° once inside the detector. All operations are performed through a glovebox installed in a Class 100 clean-room atop the detector; an automated process-control system monitors gas pressures and flow rates inside the glovebox and the connecting equipment.

Hardware. Each of the insertion rods (3.8 cm × 100 cm) is equipped with special couplers at both ends. The rods also contain a ballast wire which is sized to make the rods almost neutrally buoyant when immersed in the Borexino scintillator. A hinge in the lever arm prevents any motion over 90°, and can be used in place of any normal rod in order to facilitate longer lever arms. Figure 3 shows a map of areas that can be reached using this system.

A 1/4" diameter flexible Teflon tether tube enters the detector alongside the rods. The tether is fixed at the end of the last rod, the one holding the source, and is used to adjust the hinge angle to

2012 JINST 7 P10018

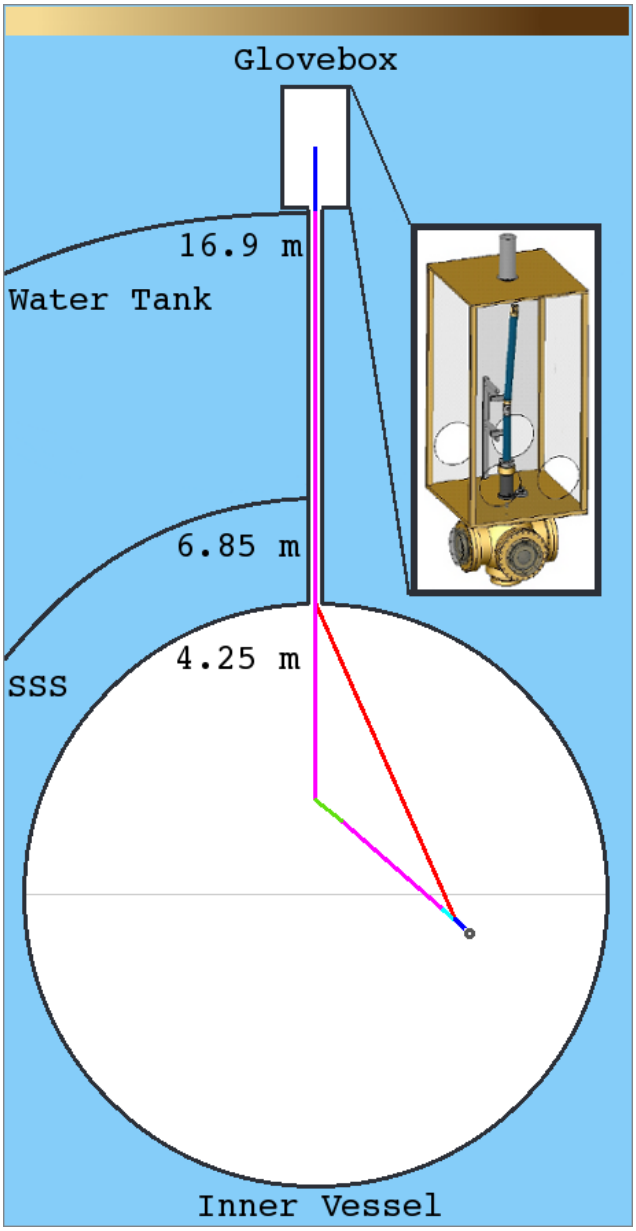

Figure 2. Schematic view of the source deployment system: the main figure shows the glovebox and Inner Vessel, together with the pipe connecting them. The inset to the right shows a zoomed view of the glovebox. In order to reach the desired location, the hinge is positioned and the system is lowered vertically into the detector. In the next step, the tether tube (red line) is withdrawn until the hinge bends to the chosen angle. To establish the azimuthal position in ϕ the rods are simply rotated $\pm 180^\circ$ — procedural limitations prohibit rotation by more than 180° in either direction. To retract the source, the procedure is reversed.

the desired position (for details see caption of figure 2). The tether also carries a fiber-optic cable that is used in determining source position (section 3.1.2). Both rods and tether are attached to a special source-coupler which holds the calibration source at its end with four spring-steel wires; figure 4 shows the assembled configuration.

2012 JINST 7 P10018

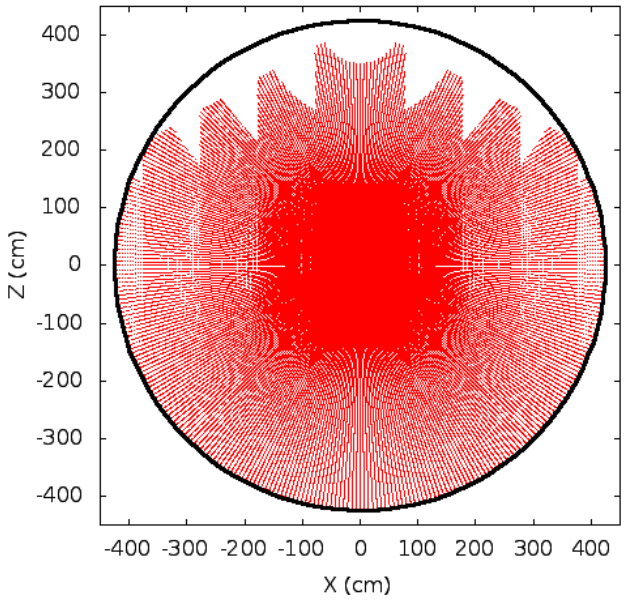

Figure 3. Schematic view of areas reachable with the Borexino source deployment system. The red points represent the mesh of positions where a source can be deployed within the scintillator volume. The black line represents the nominal position of the inner vessel.

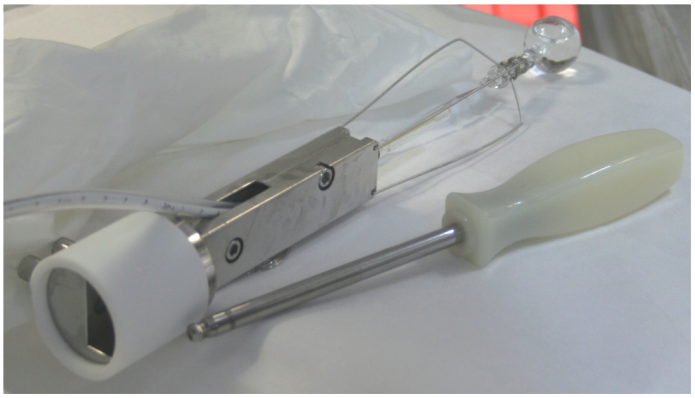

Figure 4. The special coupler used to attach the insertion rods to a calibration source and tether (entering the coupler midway down its body). A thick collar on the left hand side prevents the coupler from being drawn into the sliding seal. The four spring-steel support wires to which the source is attached are visible at the end of the coupler.

The glovebox, which also stores all of the components, remains under continued flow of low argon/krypton nitrogen ($LAKN_2$: 0.01 ppm Ar, 0.02 ppt Kr) at a pressure of 2-3 mbar. An oxygen monitor is installed in the clean-room for safety reasons, since, in case of a leak, nitrogen could exit the glove-box and displace oxygen in the clean-room. A leak in the glove-box would be dangerous for the detector as well, because of Rn, Kr, Ar, and other contaminants feeding back in the scintillator.

2012 JINST 7 P10018

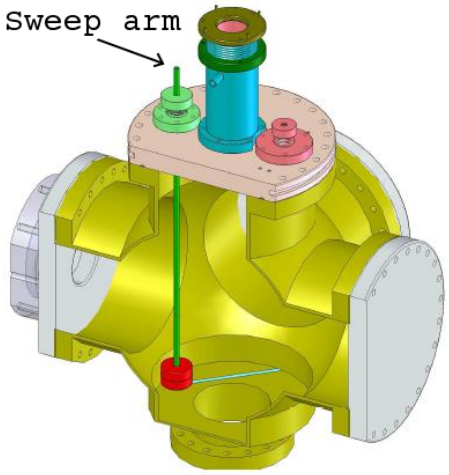

Figure 5. A six-way vacuum cross that was mounted between the glovebox and the gate valve. An additional sweep arm is used to verify the position of the rods during the source extraction.

The fluid handling system in the Borexino detector [11] requires that a slight (100 mbar) overpressure be maintained in the IV. In order to maintain this pressure while deploying sources, a 6-way cross shown in figure 5 with a sliding seal that mated around the source deployment rods at the top, was located between the glovebox and the gate valve (a diagram showing the location of the cross with respect to the glovebox is presented in the inset of figure 2). After a source was mounted and the first deployment rod enclosed within the sliding seal, the cross was brought to the necessary pressure using a flow of LAKN before the gate valve to the IV was opened.

System cleanliness. As cleanliness is the driving constraint for the system described so far, all components entering the detector (insertion rods, couplers, tether tube, and sources) have to meet the same cleanliness requirements adopted for the filling stations. The electropolished rods and couplers were placed, four at a time, into a vessel connected to the Borexino cleaning module for detergent cleaning as described in [11]. When particulate counting of the rinse water indicated a cleanliness level of Class 30 or better as defined by MIL-STD 1246C [13], the components were unloaded into a clean-room for assembly. The cross was also cleaned in the same manner because the scintillator could potentially reach this area if control of the liquid level was lost. Due to the small size of the tether and sources, these components were cleaned in ultrasonic baths prior to their usage. As shown in section 3.3.4 the effort devoted to cleaning the system allowed a successful calibration of the Borexino detector while preserving its excellent scintillator radiopurity.

Control software. Control over the system is largely performed by a custom-written program that provides a graphical-user-interface, manual and automated control over solenoid-operated components, visual and audible alarms, and data logging capability.

3.1.2 Source location system

A task of paramount importance in Borexino analyses is the definition of the fiducial volume (FV), which is directly related to the determination of the event position. Thus, one objective of the

2012 JINST 7 P10018

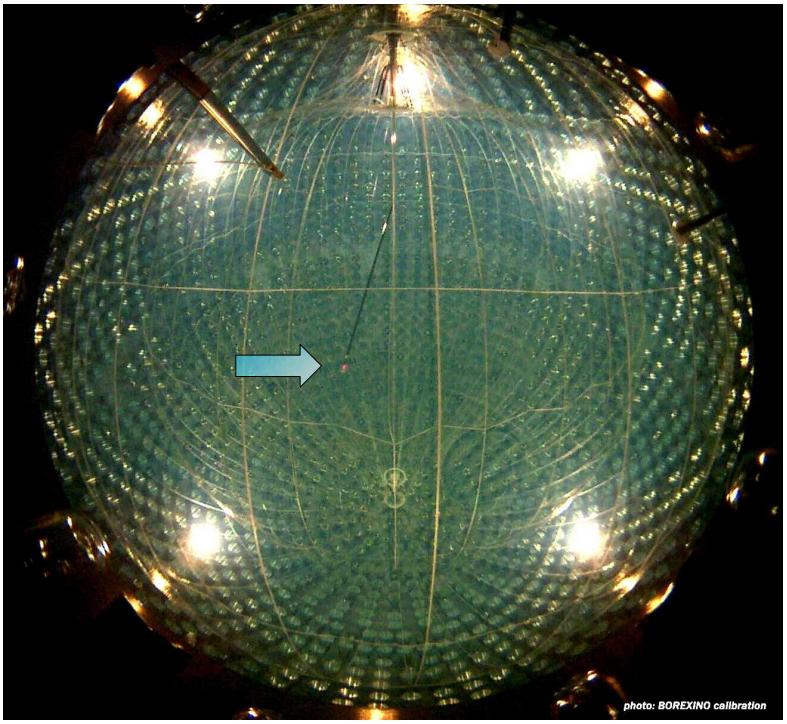

Figure 6. CCD image of the Borexino inner detector showing the insertion arm during an internal calibration. The diffuser for the location of the source is visible in red close to the center of the detector. To take this picture lights were turned on for illustration purposes. During normal calibration activities they would be off.

calibration campaigns was to study the performance of the software algorithm used to estimate the positions of data events by comparing the source locations determined using the reconstruction software with the true source locations. The method is ultimately limited by the uncertainty on the true position of the source. Achieving an uncertainty on the fiducial volume determination at the 1% level requires a precision of $\sim$1 cm on the source position determination.

The source location system consists of seven consumer grade digital cameras, six of which are on orthogonal axes. Camera 7 was installed close to the top of the detector in order to monitor for trapped gas bubbles during filling. The true location of a source can be determined in the following way: a laser-illuminated diffuser ball, attached close to the source, is flashed while the CCD cameras take pictures simultaneously. It is worth noticing that the color of the laser was selected intentionally, red light is visible in the spectrum of the cameras, but it is not harmful to the PMTs. In such a configuration, it was safe to leave the high-voltage turned on while the pictures were taken.

An example is given in figure 6. The position of the diffuser and of the source is determined via triangulation of all pictures. Although finding a point in three dimensions requires only two cameras, all seven are used to check for self-consistency and to increase the resolution of the system.

The reference coordinate system adopted throughout this paper has the origin in the SSS center and the z-axis along the vertical.

2012 JINST 7 P10018

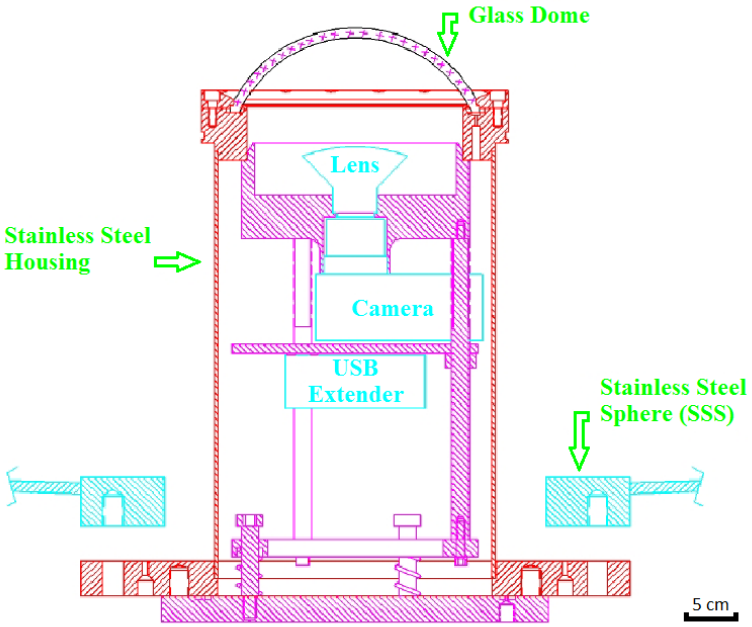

Figure 7. Assembly drawing of a camera canister. A fisheye lens was added to each assembly to yield a 183° field of view for each camera. A USB extender in each housing transmits the camera's USB signal over CAT5 cable; an analogous unit at the receiving end transforms the signal back to USB for computer read-out.

CCD cameras and computer interface. The CCD camera system employs Kodak DC290 2.4 megapixel consumer grade digital cameras, each equipped with a Nikon FC-E8 fisheye lens. The fisheye lens allows the entire IV to be viewed by expanding each camera's field of view to 183°. The camera + lens system is mounted in a housing on the SSS, with a glass underwater photography dome on the front side. Figure 7 illustrates the camera housing and the mounting design.

The cameras are controlled over an interface with the camera control box. This box houses relays and circuitry to ensure synchronized photo-taking. Additionally, the camera housing can be flushed with nitrogen in order to remove unwanted water residuals or scintillator vapors.

There are also four pin-hole LEDs present within each of the camera housings to provide fixed reference points for evaluating time stability of the location system. In addition, the pin-hole lights are visible to the same camera they are mounted with, and are used to correct motions in that camera's lens. Including the light diffuser mounted above the source, there are a total of 29 red light sources in fixed locations about the SSS that are flashed when a photo is taken to provide reference positions. Tests were performed with high voltage of all PMTs turned on, and an increase in the dark rate for illuminations as long as two seconds was not found. During normal calibration operations, photos are only taken when the DAQ has been stopped (but with the PMT high voltage still on).

A total of eight 50 W quartz-halogen lights, split into two independently wired banks, are installed in each camera housing to illuminate the detector for vessel monitoring. As a safety

2012 JINST 7 P10018

precaution, the lights are enabled with a key switch; the switch also disables the PMT high voltage. This interlock method ensures that the PMTs will never be exposed to the intense halogen light while the high voltage is on. The camera control box also contains a timer circuit which shuts the lights off after two seconds to prevent excessive heating of the housing.

The source location system must comply with the stringent radiopurity requirements of the Borexino apparatus. In particular, since the system components are installed on the SSS, we have ensured that their activity is low in comparison with the other sources of external background located at the same radial distance, like the PMTs, the light concentrators and the SSS itself. The ^{238}U and ^{232}Th concentration in the location system was measured to be negligible in comparison with that of the PMTs [14]. The contamination of ^{40}K was found to be higher than in the PMTs by about 85%. This was considered acceptable, since it accounts for a relatively small fraction (9%) of the total external background rate in Borexino.

Image reconstruction. Triangulation of the diffuser is achieved by projecting a ray in space from each camera to the diffuser, and then finding the intersection of the seven rays. In order to find a ray from one camera, it would be necessary to track the light through the camera's lens system, which not only requires detailed information about the lenses, but also a precise measurement of the camera's mounting position and direction. To overcome these difficulties, the image reconstruction process employs a transformation method that corrects for lens distortions [15], camera mounting uncertainties, and performs the correct 3D mapping of the detector onto the CCD. The transformation process uses thirteen parameters which are determined by fitting the well-known spatial coordinates of the PMTs in images of the detector taken with the lights on, as will be described later.

Camera calibration. During normal operation, the camera system uses the parameters mentioned in the previous paragraph coupled with an image to determine the position of an object in that picture. However, this process requires *a priori* knowledge of the calibration parameters. Obtaining the calibration parameters can be accomplished by effectively running the method in reverse, and using the *known* positions of the inner detector PMTs to determine the *unknown* calibration parameters.

The calibration process begins by creating an idealized picture — ellipses to represent the edges of the PMT light concentrators and μ-metal shielding — of what each camera would see and then overlaying this idealized picture onto an actual photo taken with the cameras. A user can then drag the overlay image until a given PMT on the overlay lines up with one in the actual image; the point is then saved, and the process is repeated for 100 or more points. At the end of this process, a χ^2 minimization is performed to determine the calibration parameters that would produce a corrected image lining up with the overlay. At the conclusion of this process, the thirteen parameters resulting from the calibration allow the corrected images to be treated as if they were taken by an ideal camera, vastly simplifying ray-tracing.

Position uncertainty. In order to estimate the uncertainty on the determination of the source position by the source location system, we performed several tests. First, we verified that the detector center as determined by the cameras coincides with the nominal center, derived assuming a perfectly spherical SSS. This was done by verifying that each camera ray that traverses the center

2012 JINST 7 P10018

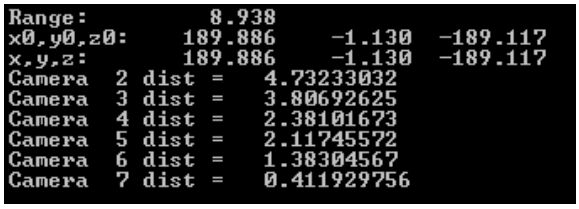

Figure 8. A view from the software window indicating the reconstructed source position (in cm) and shortest distances to each of the rays (in pixels). An approximate conversion at the center of the detector is about 1 cm = 1 pixel.

of the SSS at (0,0,0) cm also points at the center of the opposite camera across the detector. Next, using a fixed reference point in the glovebox, we obtained the absolute scale by comparing the reconstructed LED position with the total length of the rods for different locations along the z-axis (maximum uncertainty on the length of the rods is ± 0.2 cm). In this way we derived an uncertainty for the determination of the z position of ~ 0.6 cm. Even though this test was performed only on the z axis, it can be safely extrapolated to other positions, since the cameras are not located in any special orientation with respect to the z-axis.

As an additional check, the camera reconstruction software gives us the opportunity to verify how far each of the rays was from the calculated position. As an example, figure 8 shows the reconstructed position for one of the sources with calculated distances to each of the camera-rays. Six out of seven installed cameras identified this source correctly however, cameras 2 and 3 could be eliminated due to higher than expected distance, 4.7 and 3.8 pixels respectively.[1] The position was afterwards re-calculated without including these two cameras. This procedure has been adopted for the determination of all source positions and improved the reliability of the result. It was also used to investigate possible systematics of the location system connected to the source position: no directionality or radial dependence was identified.

3.2 Calibration sources

As shown in table 1, sources of different types were needed to cover the energy region of interest for Borexino and to investigate the scintillator response to different ionizing particle types. A detailed description of each of the sources is presented in the following sections 3.2.1 to 3.2.4.

With the exceptions of the neutron and laser sources, the sources were dissolved in either Borexino scintillator or water and sealed within 1" diameter quartz vials with a total volume of $\sim$6 ml. The neck of the vial had a graded transition to Pyrex glass for sealing purposes. After loading the vial with a radioisotope, the vial was frozen in liquid nitrogen, evacuated and flame-sealed. For instance, a close-up photo of the ^{203}Hg source after being attached to the source coupler is shown in figure 9.

3.2.1 ^{222}Rn and ^{14}C Sources

The vast majority of the calibration points were obtained with a compound ^{14}C-^{222}Rn source which provides α, β, and γ radiation across a large energy region. In this source, ^{14}C and ^{222}Rn were simultaneously present in the scintillator.

[1] The view from camera 1 was possibly shadowed by the calibration rods and hence, was not included in the reconstruction at all.

2012 JINST 7 P10018

Table 1. Radioactive sources used during the Borexino internal calibration campaigns. The radionuclides, energies and emitted particle types are shown in the first three columns. The fourth column indicates the positions where the sources were deployed within the scintillator. The main purposes for the individual source measurements are summarized in the fifth column. The last column indicates in which campaign the sources have been deployed: I (October 2008), II (January 2009), III (June 2009) and IV (Jul 2009), see text for more details.

Source	Type	E [MeV]	Position	Motivations	Campaign
^{57}Co	γ	0.122	in IV volume	Energy scale	IV
^{139}Ce	γ	0.165	in IV volume	Energy scale	IV
^{203}Hg	γ	0.279	in IV volume	Energy scale	III
^{85}Sr	γ	0.514	z-axis + sphere R=3 m	Energy scale + FV	III,IV
^{54}Mn	γ	0.834	along z-axis	Energy scale	III
^{65}Zn	γ	1.115	along z-axis	Energy scale	III
^{60}Co	γ	1.173, 1.332	along z-axis	Energy scale	III
^{40}K	γ	1.460	along z-axis	Energy scale	III
^{222}Rn+^{14}C	β,γ	0-3.20	in IV volume	FV+uniformity	I-IV
	α	5.5, 6.0, 7.4	in IV volume	FV+uniformity	
^{241}Am^{9}Be	n	0-9	sphere R=4 m	Energy scale + FV	II-IV
394 nm laser	light	-	center	PMT equalization	IV

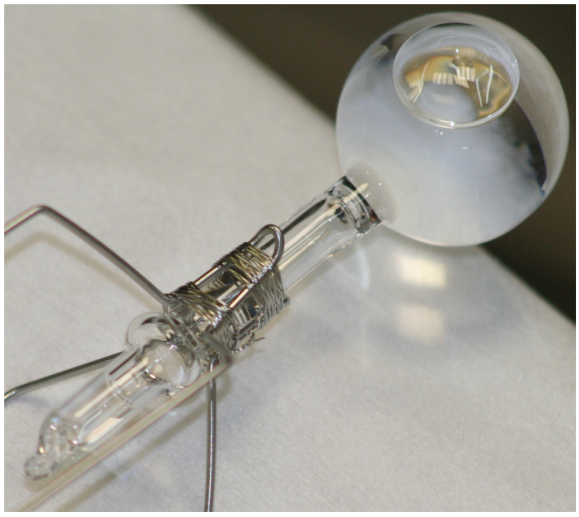

Figure 9. The ^{203}Hg γ source that was deployed in June, 2009. The spherical vial is made of quartz, whereas the neck is a graded transition from quartz to Pyrex. The rounded bulge in the neck is a safety feature to prevent the source from slipping out. Source retention is provided via the two independent wrappings with thin-gauge stainless steel wire.

Loading the vial with radon is accomplished via a calibrated flow-thru ^{222}Rn source typically used for calibration of radon detectors. A source vial is evacuated and placed in a liquid nitrogen bath while a flow of radon-loaded nitrogen gas is established through the vial. Radon, whose

2012 JINST 7 P10018

melting point is at 202 K, freezes out onto the surface of the vial maintained at 77 K, while the carrier gas continues unaffected. After an appropriate build-up time has elapsed, the gas flow is ceased, the vial evacuated and warmed up. Finally, the vacuum in the vial is used to extract scintillator from a sparging flask until the vial is completely filled.[2]

After this operation ^{14}C is loaded by using a ^{14}C-toluene solution typically used for calibrating liquid scintillator detectors. The solution was pipetted into the source vial filled with Rn-loaded scintillator. Since toluene (methylbenzene) is chemically very similar to pseudocumene (trimethylbenzene) and homogeneously miscible, ^{14}C is uniformly distributed throughout the vial.

The ^{14}C-^{222}Rn sources used in the calibrations were prepared at Virgina-Tech with an initial activity of $\sim$100 Bq. They were deployed in more than 200 positions within the scintillator (see section 3.3.2).

^{14}C is a β emitter with an end-point energy of 156 keV suitable for low energy studies. The ^{222}Rn chain consists of three α emitters, namely ^{222}Rn, ^{218}Po and ^{214}Po, with energies of 5.5 MeV, 6.0 MeV and 7.4 MeV, respectively. Moreover, it has two β/γ emitters ^{214}Pb and ^{214}Bi which have a Q value of 1.0 MeV and 3.2 MeV, respectively.

Due to the quenching phenomenon, α particles produce less scintillator light than β particles (quenching factor $\sim$10 or more) and therefore their equivalent energy in the detector is below 1 MeV. Therefore, the compound ^{14}C-^{222}Rn source provided calibration points in the energy region between 0 and 3.2 MeV which is relevant for the main solar neutrino analyses, i.e. ^{7}Be, *pep*, and CNO neutrino rate measurements. The upper plot in figure 10 shows the spectrum of the ^{14}C-^{222}Rn source.

3.2.2 γ Sources

In order to use γ sources for energy calibration in Borexino, the sources had to be mono-energetic and the scintillation light induced by associated α or β radiation had to be suppressed. This was achieved by depositing the radioisotope of interest in a non-scintillating medium within a source vial that absorbs the α and β particles.

The isotopes of all γ sources in table 1 were commercially obtained as salts dissolved in aqueous acid solutions. Thus, a pure γ source was obtained by pipetting the appropriate amount of isotope into a vial and filling the rest with deionized water. Due to EU radiation safety rules, the specific activity of the commercially-obtained solutions was limited to 1 Bq/ml.

The activity of each of the γ sources employed in the calibrations was approximately 2 Bq. For what concerns the ^{85}Sr source, the activity was precisely measured by means of γ ray spectroscopy to provide a reference value for trigger efficiency studies (see section 5.3).

3.2.3 ^{241}Am^{9}Be Neutron Source

For ^{8}B neutrino and geo-neutrino analyses [5, 7], for studies of solar and other unknwon anti-neutrino fluxes [8], and search for solar axions [10] it is essential to have energy calibration points up to 10 MeV. In Borexino this was accomplished by a $\sim$10 Bq ^{241}Am^{9}Be neutron source that was inserted into the detector during the second and third internal calibration campaigns. As shown in

[2]The scintillator used to make the sources is taken from a sampling port on the Borexino purification system. The sample is maintained under an inert atmosphere at all times.

2012 JINST 7 P10018

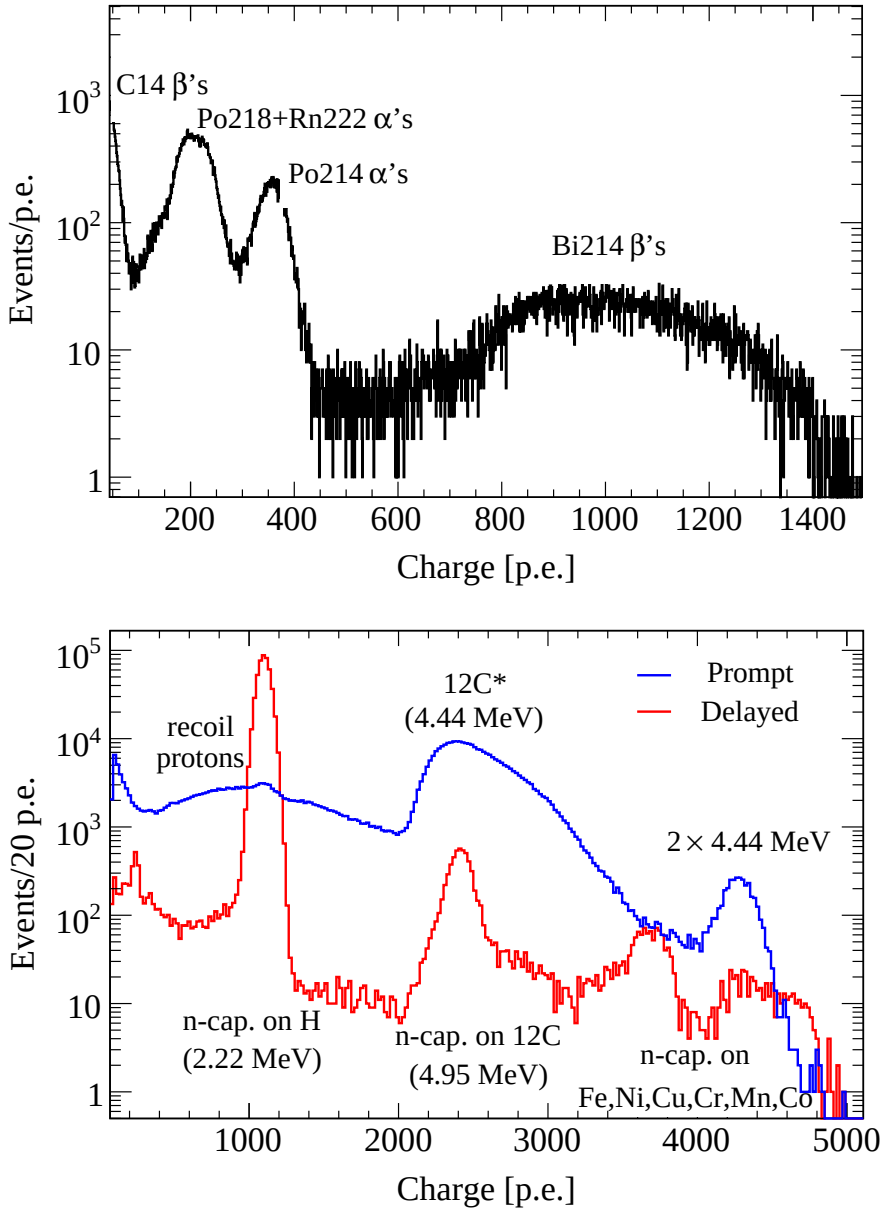

Figure 10. Energy spectrum (variable *p.e*) of the ^{14}C-^{222}Rn source (upper plot) and ^{241}Am^{9}Be source (lower plot). The ^{241}Am^{9}Be spectrum is subdivided in a spectrum from neutron-induced prompt (blue) and delayed signals (red).

figure 11, the source was contained in a 3 mm lead capsule embedded in a delrin holder to shield the 60 keV *x* rays (activity ∼180 kBq) produced by the source itself.

Neutrons are produced in two main reactions, ^{9}Be(α,n)^{12}C$_{gs}$ and ^{9}Be(α,n)^{12}C* (4.44 MeV) with energies up to 11 MeV and 6.5 MeV, respectively. The second reaction also produces one or two γ rays with a total energy of 4.44 MeV from the ^{12}C* de-excitation. These γ rays, together with the recoil protons from neutron scattering in the medium, are responsible for a prompt scintillator signal.

2012 JINST 7 P10018

Figure 11. Photo of the encapsulation in which the Borexino $^{241}Am^{9}Be$ neutron source was placed. Note that the neck contains the same mounting features as the regular source vials.

Afterwards, neutrons thermalize in the hydrogen-rich organic liquid and are captured either on protons or carbon nuclei in the scintillator emitting characteristic 2.22 MeV and 4.95 MeV γ rays, respectively. These characteristic γ rays produce a delayed signal in the scintillator according to the neutron capture time of $\sim$254 μs in pseudocumene [16]. In addition, neutrons are captured on iron, nickel and chromium nuclei of the stainless steel source insertion arm resulting in the emission of γ rays with energies up to 9.3 MeV. The lower plot in figure 10 shows the energy spectrum of both the prompt and delayed signals produced by the $^{241}Am^{9}Be$ source.

3.2.4 Laser source

During the third internal off-axis calibration campaign and during a 1-day run in September 2009 a 394 nm laser was used to provide pulsed light to a diffuser ball located at the center of the detector. The diffuser was similar to the one used by the source location system, but was designed on purpose to provide better light uniformity. The primary goal of the laser source calibration was to check the PMT time synchronization independently from the main equalization system. The standard PMT equalization is performed routinely by means of a multiplexed optical fiber system which delivers the laser light directly and simultaneously on each photocathode (more details of this system can be found in [17]). During the laser source calibration runs, the laser and the detector were synchronously triggered at 50 Hz at several different laser intensities.

3.3 Internal calibration campaigns

3.3.1 Goals

The internal source deployment and location systems described in the previous section were used in four calibration campaigns between 2008 and 2009: one on-axis campaign with modified hardware in October 2008 (I), where the sources were deployed only on the vertical z-axis through the

2012 JINST 7 P10018

detector center, and three off-axis campaigns in January 2009 (II), June 2009 (III), and July 2009 (IV). The major goals of these calibration campaigns were:

- Determination of the energy scale;
- Study of the uniformity of the detector response;
- Testing the position reconstruction algorithms and study of FV systematics at different energies and for different FV cuts;
- Validation of the Borexino Monte Carlo code and of the analytical models describing the detector response that were used during signal extraction;
- Study of the detector trigger efficiency.

3.3.2 Source locations

In order to perform position studies, some of the sources were deployed in different locations throughout the scintillator volume: overall, during the four calibration campaigns twelve different sources were deployed in 295 locations. In order to study the energy scale, the eight monochromatic γ sources (see table 1) were deployed at the center of the detector and in few positions along the z-axis. Some of the sources were also deployed in other regions of the scintillator volume (mainly at larger distance from the center) in order to probe the uniformity of the trigger efficiency of the detector. A fine-grained mapping of the detector response was performed using using the ^{14}C-^{222}Rn source deployed in more than 200 positions (see figure 12).

Since the shape of the inner vessel changed significantly during the first three years of data-collection, it was important to ensure that these instabilities did not affect the optics of the detector and thus the position reconstruction performance. As a consequence, ^{14}C-^{222}Rn sources were deployed in approximately ten standard locations within the scintillator during each calibration campaign. No significant time variation of the event position reconstruction in these standard positions was observed.

Most off-axis points scanned with the ^{14}C-^{222}Rn source were located at three equidistant ϕ values ($\Delta\phi$=120°) for a given (R, ϑ) pair. However, a more fine-grained mapping ($\Delta\phi$=30°) was performed on the equatorial plane to study possible biases present in the ϕ coordinate. Since Borexino approximately employs a spherical FV cut at R<3.021 m for its ^{7}Be neutrino analysis, the ^{14}C-^{222}Rn source was used to map the volume in intervals of $\Delta\vartheta$=15° and $\Delta\phi$=90°. These data were also used to map the precise radius of the FV as a function of the event energy. This was fundamental for the reduction of the systematic uncertainty on the FV (compare with section 5.2.2).

In order to perform position studies at higher energies, the custom-made ^{241}Am^{9}Be was deployed in approximately 30 positions within the scintillator.

Finally, during the last calibration campaign a pulsed laser source was employed at the center of the detector. Its main purpose was to perform an independent check of the PMT time equalization.

2012 JINST 7 P10018

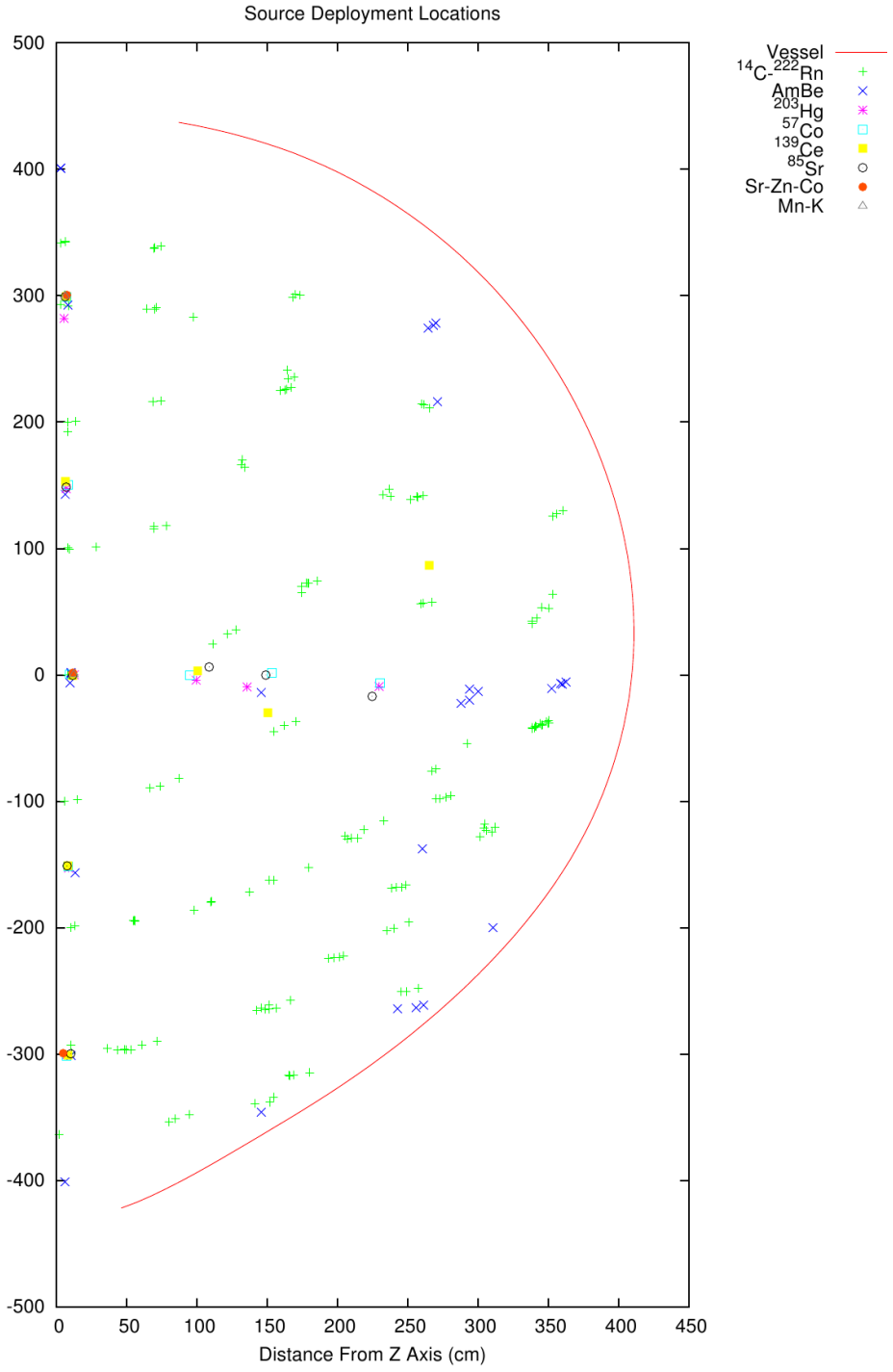

Figure 12. A map of the locations where sources were deployed during the four internal calibration campaigns. The horizontal axis corresponds to the distance from the vertical z-axis. In total, the sources were deployed in over 200 locations. Several points illustrated in the picture were also repeated at different ϕ coordinates. The red line indicates the shape of the inner vessel on January 22, 2010.

2012 JINST 7 P10018

3.3.3 Procedures

Each of the off-axis calibration campaigns lasted approximately two weeks, and involved the deployment of about five sources each time. A detailed description about it can be found in [18].

The entire process of the source removal and re-insertion takes at least two hours and for that reason all the points that required four rods below the hinge were performed first, followed by the three-rod ones, and so on. The source insertion procedure begins with the attachment of a source to the source coupler and sealing the 6-way cross. To establish an inert atmosphere in the cross, it is evacuated and then backfilled with $LAKN_2$ at least eight times. Once the required pressure and cleanliness are established, the insertion begins after opening the gate valve. When the source is finally deployed at a given position within the inner vessel, a photo is taken to confirm its position. This process is repeated for each rod inserted or retracted. Once the hinge has reached its desired position along the z-axis, the rod depth is locked with a special clamp and the ϕ angle is set. Next, the program calculates the amount of tether that needs to be extracted in order to establish the ϑ angle.

The source position is checked with a photo before starting data-acquisition. After the completion of a DAQ run, the location of the source is verified one more time before moving to a new position. The extraction procedure corresponds, in principle, to a reverse order of the insertion steps. However, special precautions are required to assure that the source passes the gate valve level. For this purpose, a special sweep-arm situated above the closure-path of the gate valve is used, as shown in figure 5.

3.3.4 System performance

Overall, the four internal calibration campaigns lasted for 54 days with a duty cycle of 65%.

The initial part of the first internal calibration was devoted to commissioning, including improvements on the process control system in terms of safety and stability. Moreover, the diffuser and illumination method was found to be inefficient and a more effective diffuser and laser-coupling scheme was developed for the following calibration campaigns. During the first calibration campaign, failure of one of the CCD cameras occurred. However, since the source location system was intentionally redundant, the loss of a single camera did not reduce the overall precision of the source position determination.

Preservation of system cleanliness. Even though the Borexino internal calibration system was designed and built following very strict requirements on radiopurity (see section 3.1.1), calibration activities always carry a non-zero risk of contamination. For this reason, internal calibrations were not performed at the beginning of Borexino data-acquisition, but after more than one year, when a significant sample of good data had been collected.

The full-scale internal calibration program left no detectable evidence of impurities. This can be demonstrated by analyzing data acquired before and after each calibration campaign. In particular, the ^{238}U concentration in the scintillator can be measured by tagging the ^{214}Bi^{214}Po fast decay coincidences (τ=236.6 μs) that belong to the ^{238}U chain. Figure 13 shows the coincidence rate (Unit: events/(day$\times$100 ton)) as a function of time, after applying the same fiducial volume cut used in the ^{7}Be neutrino analysis (R<3.021 m; $|z|$<1.67 m). The red lines mark the beginning

2012 JINST 7 P10018

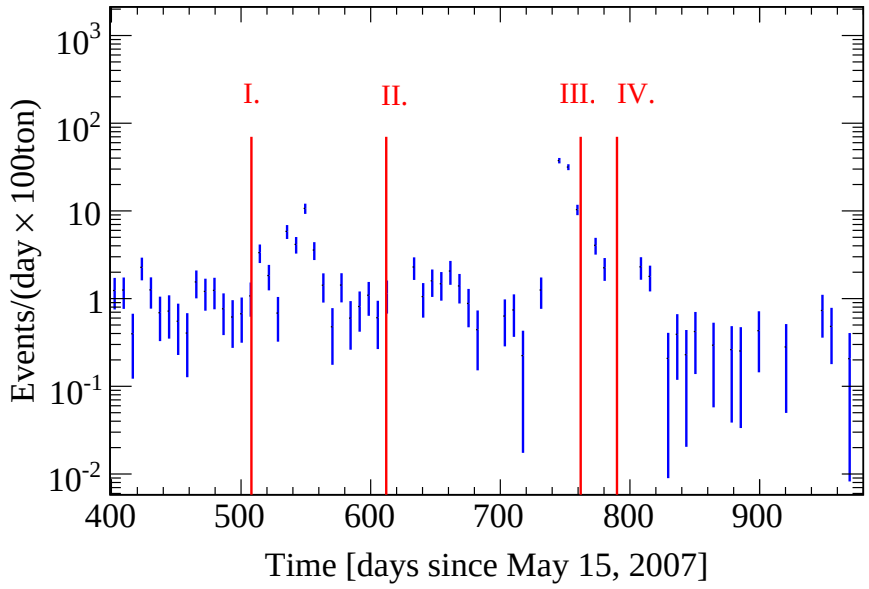

Figure 13. Rate of ^{214}Bi^{214}Po coincidences in the FV as a function of time. The peaks corresponds to Radon spikes during operations. The red lines mark the time when the four internal calibration campaigns were carried out.

of each calibration campaign. No evidence for an increase in the ^{238}U contamination due to calibrations is found. Several transient spikes in the coincidence rate can be observed. They are due to the insertion of Radon during operations (including calibrations) performed on the detector. Since Radon decays fast (τ=5.48 d) this does not affect the long-term scintillator radiopurity[3]. From the coincidence analysis, the ^{238}U concentration before and after the campaign of calibrations is estimated to be $(5.0\pm0.9)\times10^{-18}$ g/g and $(3.2\pm0.7)\times10^{-18}$ g/g, respectively.

Similarly, the ^{232}Th concentration can be investigated by looking at the fast ^{212}Bi^{212}Po coincidences. As before, this analysis shows no evidence for an increased ^{232}Th contamination. Indeed, the overall contamination in ^{232}Th before and after all four internal calibrations was found to be $(3.0\pm1.0)\times10^{-18}$ g/g and $(5.0\pm1.5)\times10^{-18}$ g/g, respectively.

One of the most dangerous background for the ^{7}Be neutrino analysis is ^{85}Kr, a β emitter with a Q value of 687 keV. This isotope can also decay with a very small branching ratio (0.43%) into a metastable state of ^{85}Rb, which de-excites emitting a characteristic 514 keV γ ray after $\sim$1 μs. This rare coincidence tag can be used to evaluate the ^{85}Kr concentration in the scintillator. Since the number of such coincidences is minimal, i.e. a few events within a year of data-acquisition, this method cannot be used to evaluate the impact of each single calibration campaigns. However, the coincidence analysis was able to show that the ^{85}Kr contamination before and after the four calibration campaigns remained constant within its total uncertainty budget.

[3]Build-up of ^{210}Pb (and therefore ^{210}Bi) due to the transient Radon spikes is expected to be negligible ($<$ 2 counts/day/100tons) given the small amount of Radon inserted. Indeed the count rate before and after calibrations in the energy regions which would be affected by ^{210}Bi has remained constant as shown in figure 14.

2012 JINST 7 P10018

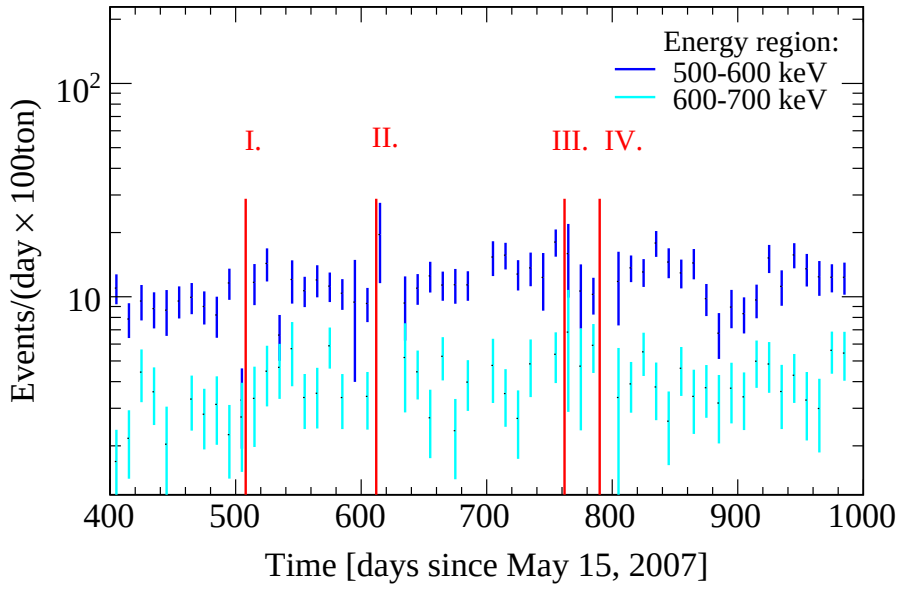

Figure 14. Count rate in the energy region between (500-600) keV and (600-700) keV as a function of time. The start of data-collection in Borexino was May 15, 2007. The red lines mark the time period when the four internal calibration campaigns were carried out.

Concerning other contaminants affecting the solar neutrino analysis, a study was performed on the stability of the count rate in two energy regions, namely (500-600) keV and (600-700) keV. These energy regions are relevant for the ^{7}Be as well as for the *pep* and CNO neutrino analyses. Approximately 55% of the count rate in the first window is due to ^{7}Be neutrinos, while the remaining 45% is due to ^{85}Kr and ^{210}Bi, a β emitter with an end-point energy of 1.16 MeV. In the second energy window around 40% of the count rate is due to ^{7}Be, CNO and *pep* solar neutrinos, while the remaining counts are due to ^{210}Bi decays. Figure 14 shows the count rate in the FV defined for the ^{7}Be neutrino analysis as a function of time. The rates for both energy windows are shown in dark and light blue, respectively. The plot shows no evidence for an increase of the counting rates due to the calibration campaigns.

In summary, the Borexino internal source deployment system has functioned as designed, by deploying a number of different sources at more than 200 locations within the IV, without leaving any detectable radioactivity in the scintillator.

4 External source calibration

In addition to the invasive internal calibration system described in the previous section, the Borexino detector is equipped with a second non-invasive calibration system, used to deploy γ sources in the outer buffer region. The goal of this system is to study the spectral shape and the radial dependence of the external background events caused by radioactivity in the outer detector components, such as PMTs, light concentrators, stainless steel sphere and so on. The most important external background in the Borexino analysis is the 2.615 MeV γ rays produced in decays of ^{208}Tl. Since

2012 JINST 7 P10018

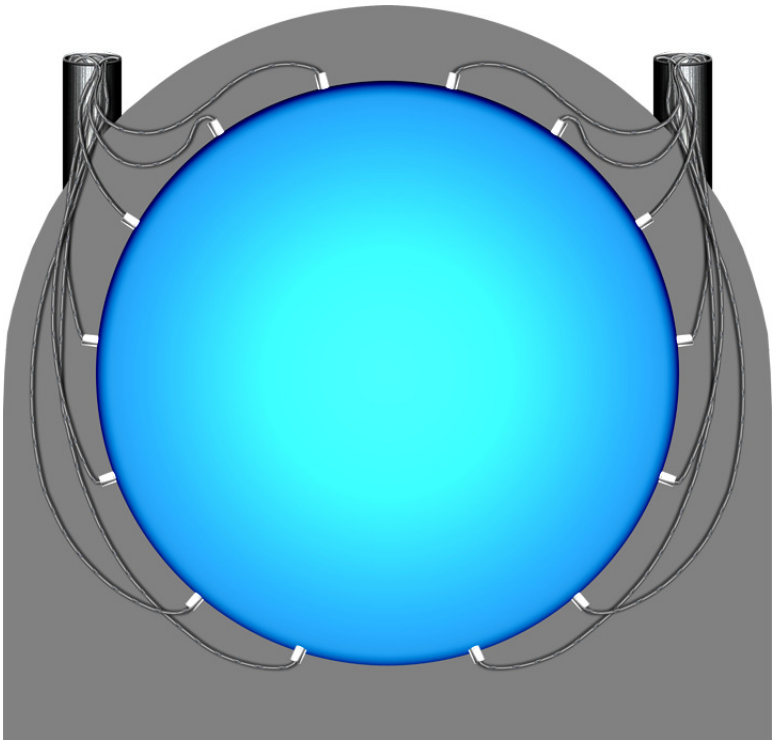

Figure 15. The geometry of the external source insertion system. Polyethylene tubes (grey) connect the top of the detector to fourteen reentrant tubes mounted on the SSS (blue) and terminate at the same depth as the PMTs at a distance of 635 cm from the center of the detector. A small γ source can be placed inside of a specially designed capsule attached to an electrician's fish tape and fed down through the tubing to the end of a reentrant tube. More details about this calibration system are summarized in the text.

these γ rays cannot be easily tagged and discriminated, they can severely affect the outcome of physics results (see, for instance, [5, 6]).

Section 4.1 describes the hardware of the external calibration system, while section 4.2 discusses the custom-made ^{228}Th source used for the two external calibration campaigns. Section 4.3 gives details on the procedures adopted during the calibration operations. The external calibration campaigns provided information not only on the external background, but also on global detector properties. This is shown in section 5.

4.1 Hardware

The external calibration system consists of fourteen 61 cm long reentrant tubes mounted at different positions along a vertical plane on the stainless steel sphere. The reentrant tubes are connected with flexible polyethylene tubing going through the water tank and ending in an organ pipe on the top platform of the detector. Figure 15 illustrates the geometry of the system. It allows to position the source at the level of the PMTs to a minimal distance of $\sim$635 cm from the center of the detector. The tubes are thick enough to withstand the buoyant forces to which they are exposed due to the presence of water in the outer detector. Additionally, the inner surface of the tubes was made smooth in order to reduce friction when a source is moved through it.

2012 JINST 7 P10018

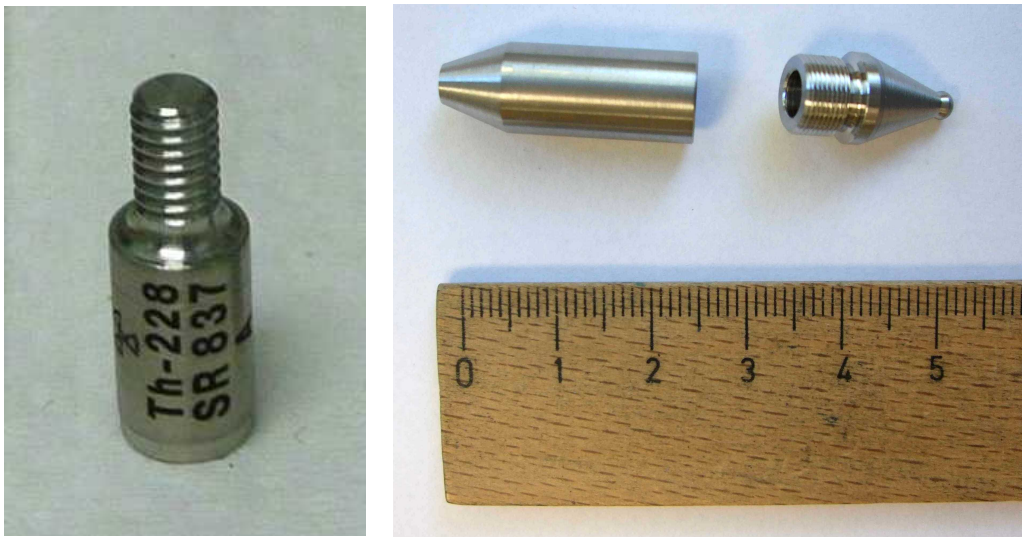

Figure 16. Custom-made ^{228}Th source (left) and capsule (right) for holding the source to be deployed by the external source system. The left edge of the capsule is silver-soldered onto a metal electrician's fish tape and then pushed through one of fourteen tubes until reaching the buffer region in the inner detector. Units of the capsule are given in centimeters.

The external source deployment begins with placing the source inside a specially designed capsule shown in figure 16. The capsule is made of stainless steel and is silver-soldered to a metal electrician's fish tape. The diameter of the capsule is 9 mm. The capsule is wrapped in electrical tape and the fish tape is then fed into the polyethylene tube until it reaches the end of the reentrant tube on the sphere. A completed insertion is verified with a closed circuit between the fish tape and the flange on the organ pipe, i.e. the circuit is established when the end of the metallic capsule touches the end of the reentrant tube. Based on this reference point it is also possible to move back the source within the reentrant tube to different positions that are known with an accuracy of ± 3 cm.

4.2 Custom-made 5.41 MBq ^{228}Th Source

The radioactive source that was chosen for the external calibrations of Borexino is a ^{228}Th source: ^{228}Th is a relatively long-lived nuclide (τ=2.76 y) and ^{208}Tl is one of its daughter nuclides: the emission probability of the 2.615 MeV γ energy line is 35.6%.

In order to collect enough statistics in a reasonable time frame a ^{228}Th source with an activity of several MBq was needed. Commercially available sources of such activities typically use ceramic matrix materials to incorporate the radionuclides. Depending on the chemical composition, the low-Z nuclides in the ceramics induce the emission of unwanted neutrons due to (α,n) reactions. Even though a neutron source strength of the order of 100 s^{-1} is not problematic for Borexino, strong limitations for the usage of neutron emitting sources are imposed by the LNGS underground laboratories. The reason is that neighboring experiments searching e.g. for dark matter might be perturbed by these neutrons. Due to this fact, the production of a custom-made ^{228}Th

2012 JINST 7 P10018

source with reduced neutron source strength became necessary. It was achieved by using a gold foil in which the thorium was embedded. Gold has a high (α,n) energy threshold of 9.94 MeV, while the mean energy of α particles from the ^{228}Th chain is 6.5 MeV. A detailed description of the source production and characterization is given in [19]. In summary, the final activity of the source was (5.41±0.30) MBq, while the neutron source strength was measured to be (6.59±0.85) Bq (Reference date: March 1, 2010).

4.3 External calibration campaigns

4.3.1 Goals

The external calibration system and the custom-made ^{228}Th source described in the previous sections were used in two external calibration campaigns. The main goals of these calibration measurements were:

- Determination of the spectral shape of the external 2.615 MeV γ rays for different fiducial volumes;
- Study of asymmetries in the energy response of the detector for events more distant from the detector center;
- Determination of the radial distribution of the external γ events;
- Precise determination of the inner vessel shape;
- Validation of the Borexino Monte Carlo code.

In addition, other large-scale scintillator and inner detector (ID) properties could be determined. Some of the obtained results are presented in section 5.5.

4.3.2 Procedures and system performance

The first external calibration campaign was performed in July 2010 for a period of 9.0 days with a duty cycle of 95%. At that time the activity of the source was ∼4.8 MBq. Data were collected in three different positions, two lying in the upper and one in the lower hemisphere of the detector. In one case the source was at a distance of ∼635 cm from the center of the detector, in the other two cases at ∼685 cm, i.e. close to the stainless steel sphere. During the calibration campaign, the Borexino trigger threshold was increased from ∼50 keV to ∼200 keV in order to guarantee a stable DAQ. Details are given in [20]. Moreover, the most exposed PMTs close to the source positions were tested showing no anomaly during the whole measurement despite the high trigger rate.

In order to study the properties of the external background in Borexino in more detail, a second external calibration campaign was carried out in November-December 2011. It lasted for 27.9 days and the achieved duty cycle was 80%. During this calibration campaign, a relatively low trigger threshold of ∼120 keV was adopted in order to keep the detector supernovae-live for different neutrino and antineutrino flavors [21].

At the time of the second calibration the activity of the ^{228}Th source was still ∼2.9 MBq. Data were acquired for ten different positions distributed from the top to the bottom of the detector. In

2012 JINST 7 P10018

all cases the distance of the source from the detector center was ∼685 cm. Several positions were measured twice for stability tests at the beginning and at the end of the calibration campaign. No change in the detector performance was observed.

5 Calibration results

In this section we show that the calibration systems described in section 3 and 4 have worked properly and have significantly contributed to the success of the Borexino experiment. A selection of several important issues which have been thoroughly studied using calibration data is presented. Sections 5.1 and 5.2 discuss some of the systematics studies performed using data collected during the internal calibration campaigns. Section 5.1 briefly reviews the role that calibrations have played on the energy scale determination, while section 5.2 is focused on the tests and validation of the event position reconstruction algorithm. Section 5.3 is focused on the evaluation of the trigger efficiency as a function of the reconstructed event position for energies below ∼0.5 MeV. Section 5.4 summarizes an interesting application of both the CCD camera location system and the external calibration system for monitoring the inner vessel shape. Finally, section 5.5, discusses results obtained from the external calibration campaigns such as the energy spectrum and radial distribution of external γ rays within the buffer and scintillator. Furthermore, several global detector properties derived from the external calibration data will be presented.

5.1 Energy reconstruction

In principle, the energy deposited by a particle interacting in the Borexino scintillator is proportional to the number of photons collected by the PMTs. An electron with kinetic energy of 1 MeV produces approximately 500 photoelectrons in the Borexino detector. We define here two energy estimators which will be used in the following: *p.e.*, the total number of photoelectrons collected in the acquisition gate and N_{PMT}, the number of triggered PMTs. The light production in an organic scintillator is affected by non-linear effects such as light quenching [22]. Furthermore, due to the large size of the detector, light collection is significantly perturbed by photon propagation effects like absorption, re-emission, and scattering processes. In addition, geometrical shadowing effects and an asymmetric distribution of operational PMTs have to be taken into account. All these effects can contribute to a non-uniform energy response. For these reasons, the determination of the energy scale of the Borexino detector is complex and requires Monte Carlo simulations capable of reproducing the details of the emission and the propagation of photons within the scintillator. The internal calibration campaigns were fundamental in this respect, allowing us to fine-tune several Monte Carlo input parameters like the light yield, the quenching factor k_B according to the Birks model [22], and the scintillator and buffer attenuation lengths. The energy scale determination and its uniformity will not be covered here. A comprehensive discussion, including all the details concerning the Monte Carlo code and its optimization can be found in [23]. As an example, figure 17 shows the energy spectra for the eight γ sources described in section 3.2. These sources provided eight calibration points covering most of the energy region of interest for Borexino, i.e., from as low as 122 keV (^{57}Co source) up to 2.5 MeV (sum of the two γ rays from ^{60}Co decays). This was essential to fine-tune the Monte Carlo code which should reproduce the scintillator non-linear response over this relatively large range of energies. The plot shows the positions of the γ energy

2012 JINST 7 P10018

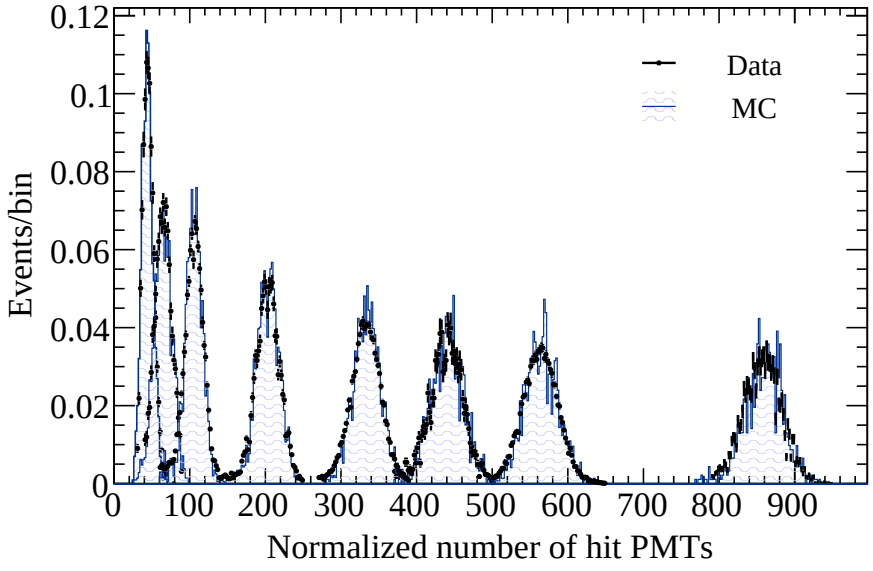

Figure 17. Energy spectra of γ lines from eight different calibration sources expressed in terms of the normalized number of hit PMTs. The peaks from left to right belong to the ^{57}Co, ^{139}Ce, ^{203}Hg, ^{85}Sr, ^{54}Mn, ^{65}Zn, ^{40}K, and ^{60}Co source. The area of a single peak is normalized to unity for a better comparison. The Monte Carlo simulated spectra are within 0.2% agreement with the measured ones.

lines obtained from the calibration data and from Monte Carlo simulations: the agreement between the two is excellent.

5.2 Position reconstruction and fiducial volume

5.2.1 Position reconstruction: algorithm and effective index of refraction

The reconstruction of a physics event position $\vec{r}_0$ in Borexino is based on the time distribution of the collected photons: the algorithm considers for each photon its arrival time t_i and the position $\vec{r}_i$ of the PMT which detected it, subtracts its time-of-flight T^i_{flight}, and compares the photon time distribution with the reference probability density function (*pdf*) of the Borexino scintillator (figure 18). The event position is calculated by maximizing the likelihood $L_E(\vec{r}_0, t_0 \mid (\vec{r}_i, t_i))$ that the event occurs at the time t_0 in the position $\vec{r}_0$ given the measured hit time pattern $(\vec{r}_i, t_i)$.

Note that the shape of the *pdf* depends on the charge q collected at each PMT (figure 18). For events with energy deposition below 1 MeV most of the PMTs work in the single-photon regime, while at higher energies or close to the borders of the IV this is no longer the case, and the multi-p.e. effect has to be taken into account to avoid bias in the reconstruction.

During the iteration of the minimization process the time-of-flight T^i_{flight} of each single photon is calculated by

$$T^i_{\text{flight}}(\vec{r}_0, \vec{r}_i) = \frac{|\,\vec{r}_0 - \vec{r}_i\,|}{v_g} \tag{5.1}$$

2012 JINST 7 P10018

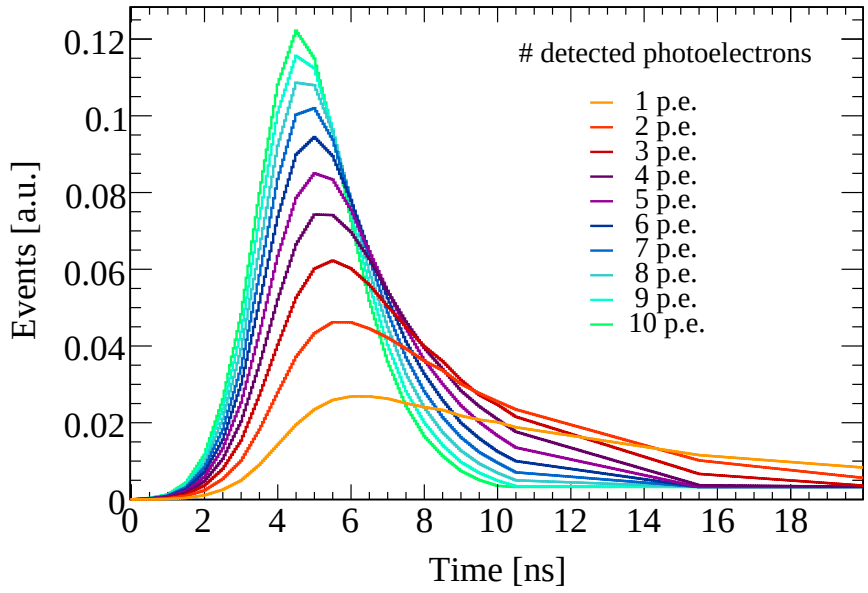

Figure 18. Distributions of times at which the first photo-electron (p.e.) from an event is detected by one of the Borexino PMTs, after time-of-flight subtraction. By comparing the probability density functions (*pdf*s of events, where either a single p.e. or multiple p.e. are detected, the time-of-arrival of the first p.e. is pushed to earlier time in the latter cases. These distributions are used as *pdf*s in the position reconstruction software algorithms.

where $\vec{r}_i$ are the coordinates of the PMT that has detected the *i-th* photon. The parameter v_g corresponds to the group velocity of the wave packet emitted in the scintillation event

$$v_g = \frac{c}{n - \lambda \cdot dn/d\lambda} \tag{5.2}$$

In the region of interest for Borexino, between approximately 350 and 600 nm, the variation of n as function of λ is relatively small ($\simeq$3%), however it has a strong impact on the effective velocity of the propagating scintillation wave packet, as can be seen from Equation (5.2). This has to be taken into account in the reconstruction algorithm by using an effective index of refraction $n_{\rm eff}$ significantly larger ($n_{\rm eff}$=1.68) than the index of refraction of pseudocumene measured at 600 nm ($n_{\rm PC}$=1.50). Calibration data were crucial in determining the exact value of $n_{\rm eff}$ needed for a correct reconstruction of the event positions. Note that prior to the calibrations the position reconstruction code was tuned using contaminants uniformly distributed in the scintillator such ^{14}C and ^{222}Rn. At that time, the systematic uncertainty on the position reconstruction was the dominant contribution to the total uncertainty budget for the ^{7}Be neutrino measurement [2].

5.2.2 Position reconstruction using radioactive sources

The ^{222}Rn and ^{241}Am^{9}Be source data were used to estimate the quality and possible systematics of the position reconstruction performance. As pointed out in section 3.2 the two sources were placed in $\sim$ 200 and $\sim$ 30 positions within the scintillator, respectively. Figure 10 shows the energy

2012 JINST 7 P10018

spectra of the two sources in the variable *p.e.* described in section 5.1. Both sources cover most of the energy range of interest for the main Borexino neutrino analyses: the ^{222}Rn source spectrum covers the region of 0-3.2 MeV suitable for the ^{7}Be, *pep*, and CNO neutrino analyses. The prompt and delayed spectrum from the ^{241}Am^{9}Be source measurement is ideal for e.g. ^{8}B solar neutrino and for geo-neutrino studies.

As already mentioned in section 3.1.2, the nominal source position was independently measured by the CCD camera system with an uncertainty of ± 0.6 cm at 1σ. Figure 19 shows the difference between the reconstructed and nominal position for ^{214}Po events from a ^{222}Rn source measurement in the detector center: the resolution of the distribution for these events ($\sim$700 keV electron equivalent) is 12 cm (σ) for x and y and 13 cm for z.

The dependence of the position reconstruction resolution from the deposited energy is shown in figure 20 for events reconstructed at the center: the resolution for the x and y coordinates ranges from 15 cm at $\sim$150 p.e. to 9 cm at $\sim$500 p.e. The resolution of the z coordinate is $\sim$2 cm worse, since the PMT coverage in the z direction is reduced.

In order to investigate possible systematics associated with the position reconstruction, the reconstructed and nominal positions were compared for all ^{222}Rn source positions. Figure 21 depicts the difference between the mean value of the reconstructed coordinate (x, y, z) and the corresponding nominal value for all available ^{222}Rn source data. The coordinates x and y are well reconstructed, i.e., the distribution is centered approximately on 0 with a sigma of $\sim$1.5 cm and tails up to 3 cm maximum. The small bias (-0.45 cm) in y direction is negligible. Note that the CCD reconstruction uncertainty of 0.6 cm is included in the widths of the distributions in figure 21, and is not disentangled here. A more significant bias of approximately -3 cm in the reconstructed z coordinate is observed. The origins of this effect have not yet been understood: it may be the result of a small offset in the position of the PMT coordinate system. Nevertheless, as pointed out in the following section 5.2.3 the observed z-shift negligibly contributes to the systematic uncertainty in Borexino physics results.

The performance of the position reconstruction as a function of position and energy was studied using both ^{222}Rn and ^{241}Am^{9}Be source data. Figure 22 shows the difference between the reconstructed and nominal coordinates as functions of the coordinate itself for ^{214}Po events. Biases in the reconstruction would show up in non perfectly flat distributions. The plot shows that the coordinates x and y are well reconstructed at all energies, while the z coordinate is not flat near the detector poles and exhibits the already mentioned shift downwards. Irregularities in the polar regions are due to shadowing effects of the IV plates that reduce the light collection. Since typical fiducial volumes in Borexino exclude events reconstructed in the polar regions where the external radioactivity contribution is higher, this effect has no impact on physics results.

5.2.3 Fiducial volume determination and systematics

The event position reconstruction is used to define a subregion of the active volume called the fiducial volume (FV) via offline software cuts. The FV determination allows us to efficiently exclude the high radius background events emitted from detector materials surrounding the radiopure scintillator. Since these background events have different radial penetration depending on their energy, the FV definition depends on the energy region of interest for a given neutrino analysis. The FV definition introduces an uncertainty in the target mass and, thus, in the neutrino rate determination.

2012 JINST 7 P10018

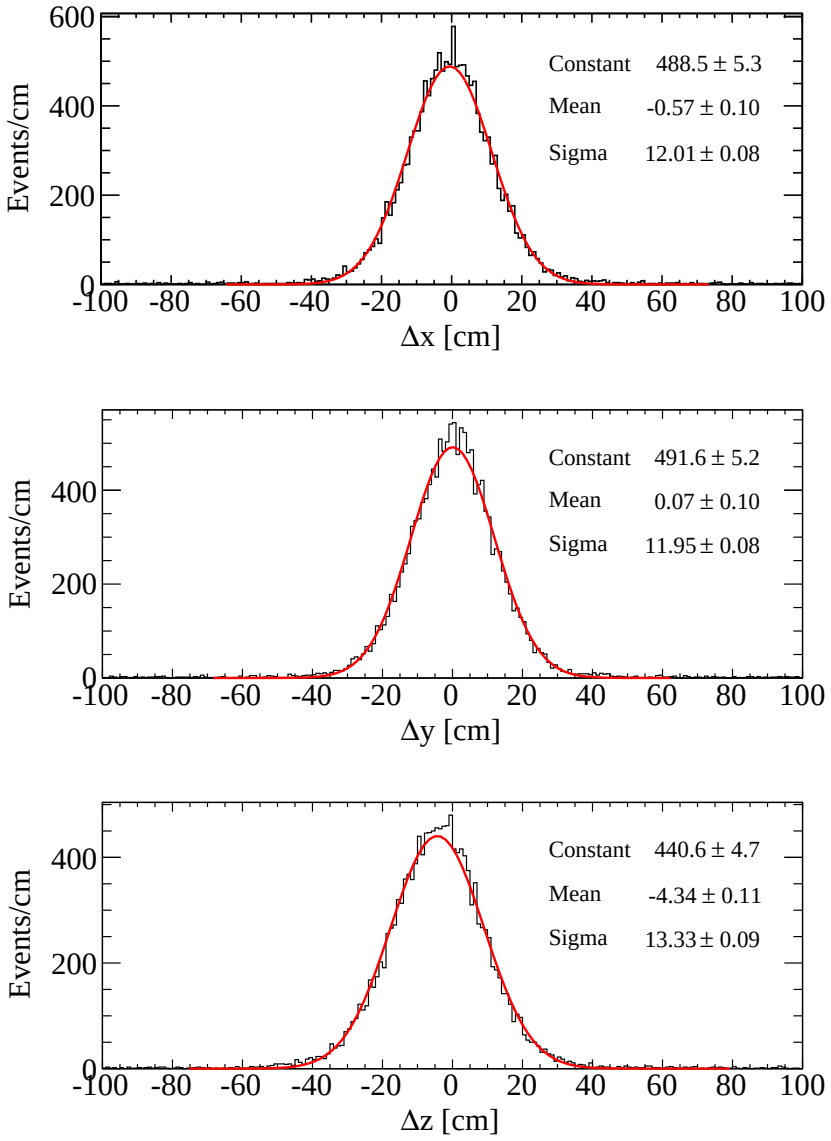

Figure 19. Difference between the coordinates x, y and z reconstructed by software algorithms versus the nominal ones using the CCD camera calibration system. The events used for the comparison are ^{214}Po events emitted from a ^{222}Rn calibration source placed at the center of the detector.

Calibration data were used to evaluate the systematic uncertainty associated with the FV selection for the different neutrino analyses. For instance, the FV used in the ^{7}Be neutrino analysis is defined by a radial cut R<3.021 m and a z-cut of $|z|$<1.67 m [3]. In order to estimate the systematic uncertainty on the fiducial mass, source data corresponding to positions at the border of the ^{7}Be FV were selected. For this data set, the distributions of ΔR and Δz, i.e. the difference between reconstructed and nominal value of the radius and of the z coordinate, were calculated. The FV systematic uncertainty was estimated by comparing the nominal value (86 m^3) with the values obtained by varying

2012 JINST 7 P10018

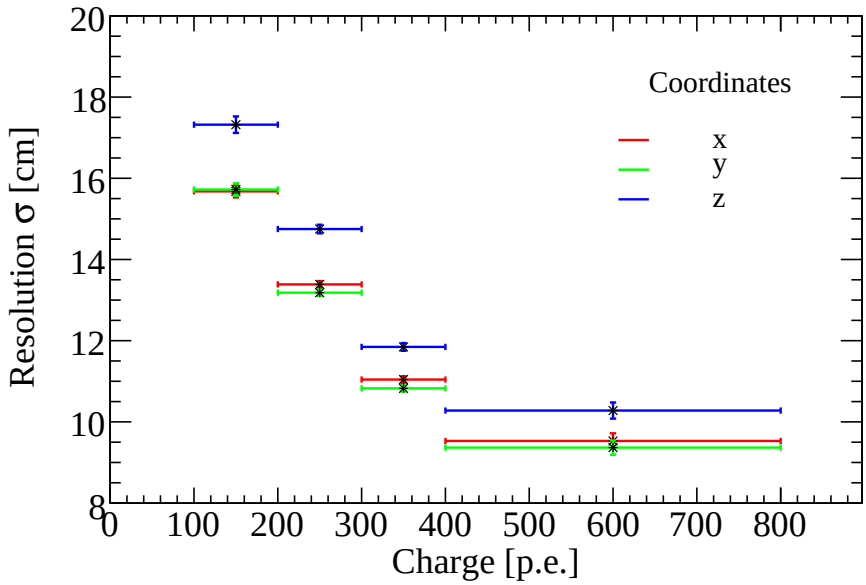

Figure 20. Resolution σ for the three coordinates x, y and z as function of the collected charge (unit: number of photoelectrons). The results are based on calibration data from the ^{222}Rn and the ^{241}Am^{9}Be source placed in the detector center.

R and z between the minimum and maximum ΔR and Δz. Based on this, the FV contribution to the total systematic uncertainty budget of the ^{7}Be neutrino rate is +0.5% and -1.3%. The systematic shift of 4 cm in the z direction (section 5.2.2) has a negligible impact on the selected FV, i.e. less than 0.01%.

5.3 Trigger efficiency

In addition to energy calibration and FV studies, the ^{85}Sr source discussed in section 3.2 was also used for efficiency studies. We know from an independent work performed with laser light, that the trigger efficiency is >99.999% for energies greater than ∼120 keV. This result was obtained exploiting the PMT equalization system [17] which provides pulsed laser light of known intensity simultaneously to all the photomultiplier tubes. A similar study can be performed with a radioactive source of known activity. An advantage of this method is that it allows us to study the detector efficiency as a function of position, by deploying the source in critical points within the scintillator, for example at the borders of the FV. ^{85}Sr decays with a lifetime of τ=93.54 d under emission of a characteristic 514 keV γ ray. This energy is relevant in particular for the solar ^{7}Be neutrino analysis. The activity of the source was measured with a germanium detector and found to be (3.28±0.07) Bq (reference date: June 18, 2009). The source was then deployed in eight positions, some of which at the periphery of the FV used in the ^{7}Be neutrino analysis and its activity was measured with the Borexino detector by performing a spectral fit. A spherical cut of R=1 m centered on the nominal source position was needed to reduce background from contaminants distributed in the scintillator volume, such as ^{210}Po. The detector efficiency was estimated by

2012 JINST 7 P10018

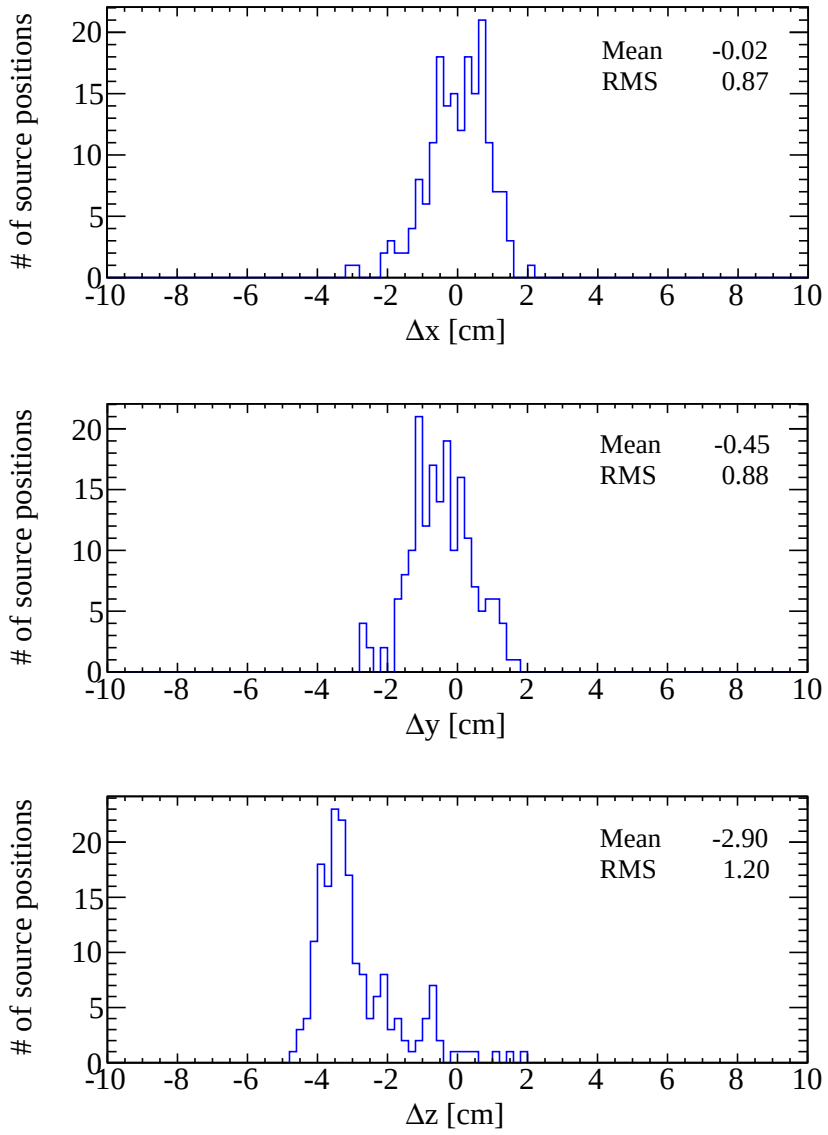

Figure 21. The ^{222}Rn source was deployed in 182 different positions within the Borexino scintillator. For each position the mean value of the event positions reconstructed by software algorithms as well as by the CCD camera calibration system was determined. The plot depicts the difference between these two values for the coordinates x, y and z.

comparing the measured activity with the nominal one and was found to be consistent with unity in all positions, showing no loss at the border of the Fiducial Volume. From this analysis we find ε(E=514 keV)=1.05$\pm$0.03 (stat) $\pm$0.03 (syst) where the systematic error includes the uncertainty on the nominal activity of the source and the systematic error associated with the cut and fit procedure applied to extract the ^{85}Sr source signal from data.

2012 JINST 7 P10018

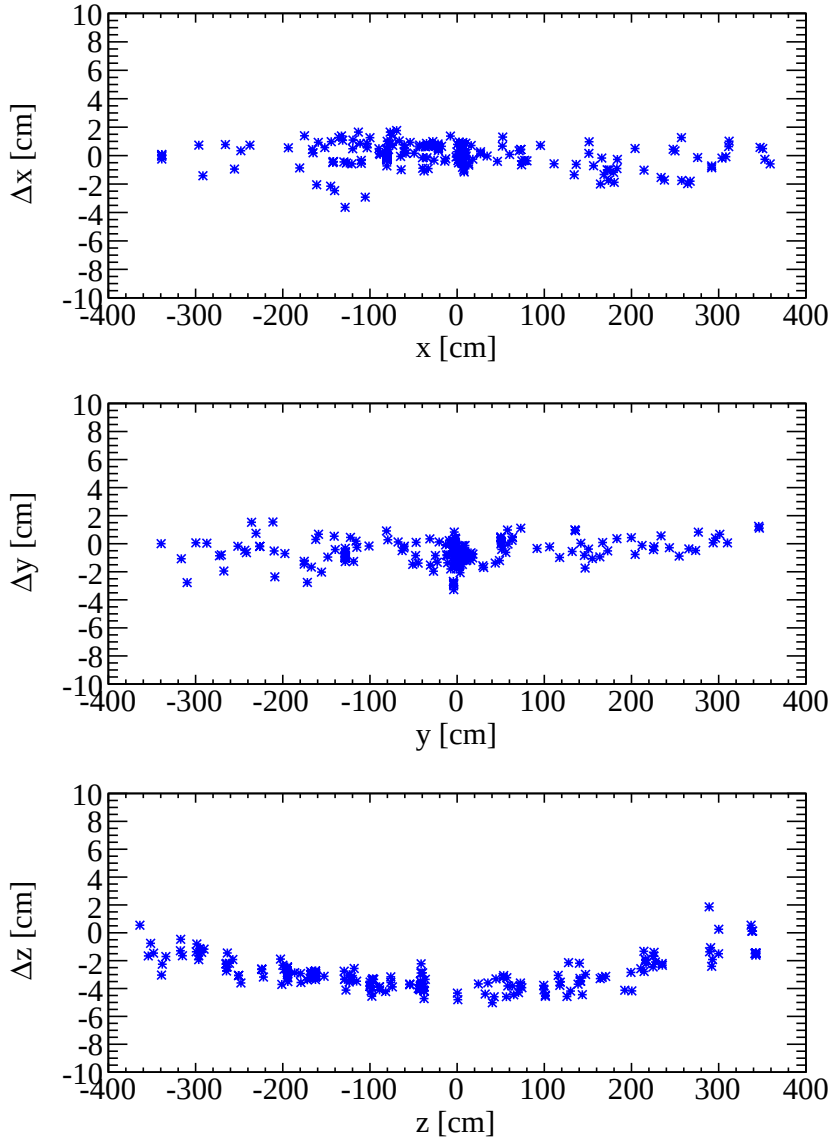

Figure 22. Difference Δx, Δy, Δz between the mean values of the ^{214}Po event position distributions reconstructed by software algorithms and by the CCD camera calibration system as function of the coordinates x, y and z.

5.4 Vessel shape analysis

The inner vessel is one of the most fragile component in the design of the Borexino detector. This very thin nylon film separates two massive, and close-to-equal in density liquids and needs to be monitored carefully. The calibration systems discussed in sections 3 and 4 provide two independent methods to determine the vessel shape.[4] These tools became particularly important in identifying a

[4] A third method for determining the vessel shape exploits the ^{210}Bi contamination of the vessel and will not be discussed here.

significant deformation of the vessel in May 2009 which was the result of a small leak of the active scintillator into the buffer.[5]

The first of the two methods used for the inner vessel shape reconstruction is given by the CCD camera system. For this purpose the high voltage of all PMTs has to be turned off and the halogen-lights switched on. Under these conditions the vessels are easily visible to the CCD cameras in most locations due to small amount of light reflected from the vessel surface facing the camera housings. Photos are taken from all the cameras to visually mark (r, ϑ) points on the edge of the vessel. Each of the points can be used to project a ray back to the camera which took the picture. This ray is, by definition, also a tangent to a sphere centered on the detector's origin. To the first order, the radius of this tangent point is the radius of the vessel at the given ϑ. The vessel profile obtained with this method can be seen in figure 23 (empty circles and empty squares) which shows the deviation dR from the nominal value of the vessel radius (R=4.25 m) as a function of the zenith angle ϑ.

The second technique relies on γ ray tomography of the nylon vessel using the external ^{228}Th source (see section 4): the nylon vessel represents the transition region between scintillator and the largely non-scintillating buffer liquid. By irradiating the vessel from the outer detector region, it is therefore possible to locate the highest-radius visible events in each direction from the detector center. For the extraction of the angular-dependent radial information the following method is applied. First, the zenith angle ϑ and the relative distance from detector center is calculated for all events induced by the external γ source. Then the radial distribution of events lying in separated slices of ϑ are plotted. An example for events collected during the second external calibration campaign with dϑ=(-50°;-55°) is shown in figure 25. Finally, the radial distributions obtained for the different slices $d\vartheta$ are fitted with a convolution of the detector response and four functions described in more detail in section 5.5.2. It turns out that only a short calibration time of one day is required in order to extract the vessel shape information with the 5 MBq ^{228}Th source: the irradiation of the inner vessel from four almost equidistant source positions around the SSS, i.e. two in the equatorial region and two in the upper and lower polar region, is sufficient for a precise extraction of the vessel shape information. Herein, the fit uncertainty of the angular-dependent radius is typically around 2 cm. Figure 23 shows the vessel profile obtained with this method (red stars) superimposed to the ones obtained with the CCD camera system before (blue circles) and after (blue rectangles) the first external calibration campaign. The results of the two methods are in good agreement.

Once the (r, ϑ) shape profiles have been recorded, an averaged curve can be computed to perform a numerical integration to determine the volume of the inner vessel. A $\pm$2 cm error on the position of an item in the detector translates to an uncertainty of approximately 1.5% on the *absolute* volume for a typical set of photos. Relative errors between two sets of photos are lower — at the level of $\pm$1 m^3 over the volume of the inner vessel, a 0.3% accuracy.

[5] After the discovery of the leak, the vessel has been refilled with scintillator and the leak rate has been reduced to tolerable levels by diminishing the difference in density between the scintillator and the buffer liquids.

2012 JINST 7 P10018

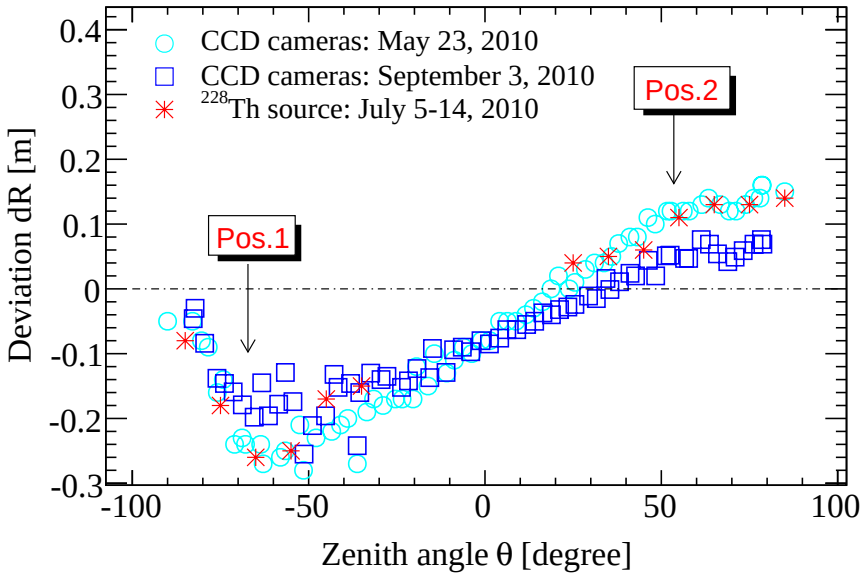

Figure 23. Comparison of the vessel shape reconstruction using the CCD camera photos and the external ^{228}Th source. The CCD camera images were taken on May 23 and September 9, 2010, while the *external calibration* data covers the period between July 5-14, 2010. The ^{228}Th source was placed only on the two zenith angles 53.5° and -67.2°, thus not all the vessel was irradiated. Both methods lead to similar results, where the nominal vessel radius R=4.25 m is deformed by as much as dR=± 0.3 m close to the poles.

5.5 External background

5.5.1 Energy spectrum of the external background

One goal of the external source calibrations was the determination of the energy spectrum of the external γ rays originating from the outer parts of the Borexino detector. This background is dominated by 2.615 MeV γ rays from ^{208}Tl decays in the detector materials surrounding the organic liquids. The corresponding energy spectrum is expected to have a radial dependence. Since Compton-scattered 2.615 MeV γ rays have a reduced probability to reach the inner core of the scintillator, the energy spectra of external background events reconstructed within small fiducial volumes (FV) around the detector center have a suppressed Compton continuum and vice versa. However, the exact shape of the Compton continuum for a given FV is *a priori* not known. The shape depends on the detector dimensions and structure as well as on the materials used. Thus, the shape cannot be deduced analytically with a satisfactory precision. The calibration with the external ^{228}Th source allowed us to reproduce the energy spectrum of external 2.615 MeV γ rays in Borexino. The obtained spectra for five different concentric FVs are shown in figure 24. Three FVs are spherical and include all events reconstructed within a radius R, whereas the FVs used for the solar ^{7}Be as well as *pep* neutrino analyses have a radial cut of R<3.021 m and <2.8 m, and a vertical z-cut of $|z|$<1.67 m and -1.8 m <z<2.2 m, respectively. Rates and spectral shapes are different. In the cases of spherical FVs with R<2.5 m and <3.0 m the rates vary from 1.3 to 4.4 events/(day×100 ton) in the energy region [0.2,3.0] MeV. The fraction of events lying below 2.0 MeV are ∼20% and ∼30%, respectively. Below 0.2 MeV the external background contribution is negligible in both FV cases.

2012 JINST 7 P10018

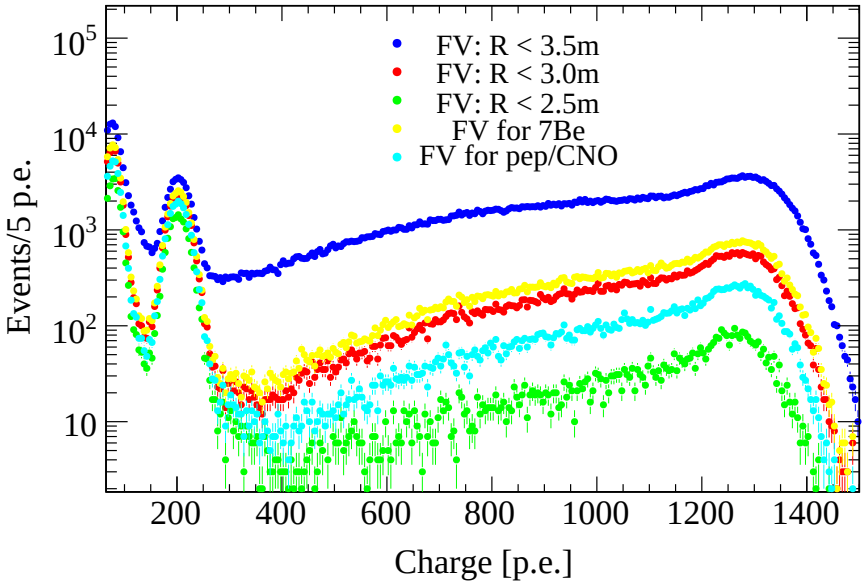

Figure 24. Energy spectra of external γ rays emitted by the ^{228}Th source for different fiducial volumes. All data acquired during the second *external calibration* campaign in different source positions were superimposed. The spectra from contaminants such as ^{14}C and ^{210}Po decays were not subtracted and are still visible at lower energies.

On the one hand, the deduced experimental energy shape is used to test the Borexino Monte Carlo code [23]. On the other hand, the data are used to study the position dependence of the energy reconstruction. Finally, the obtained external background profile can be used in global spectral fits as an experimentally known component.

5.5.2 Radial distribution of the external background

The definition of the optimal fiducial volumes in Borexino requires a precise knowledge of the spatial distribution of external background events. To a first approximation, given the spherical symmetry of the detector and since most of the external background sources are located near the SSS surface, the distribution of background events depends on radius only. Thus, the radial dependency of the external background in Borexino has been studied by means of the externally placed ^{228}Th source. The radial distribution of such events is shown in figure 25. The distribution of events reconstructed in the scintillator and buffer was fitted taking into account four components. The first component corresponds to a volumetric function. It describes the bulk contamination given mainly by ^{14}C and ^{210}Po decays that are isotropically distributed in the scintillator and represent an intrinsic background in the external calibration data. The second fit component represents the β contamination on the nylon surface of Inner Vessel. The third distribution is an exponential function. It reflects the γ rays that are emitted by the external calibration source and that are able to penetrate the scintillator volume towards the detector center. The fourth component is generated by the external source γ rays that deposit most of their energy in the buffer region where the emission of scintillation light is suppressed by more than one order of magnitude. The larger the distance of the reconstructed light baricenter from the Inner Vessel the lower its probability to be detected.

2012 JINST 7 P10018

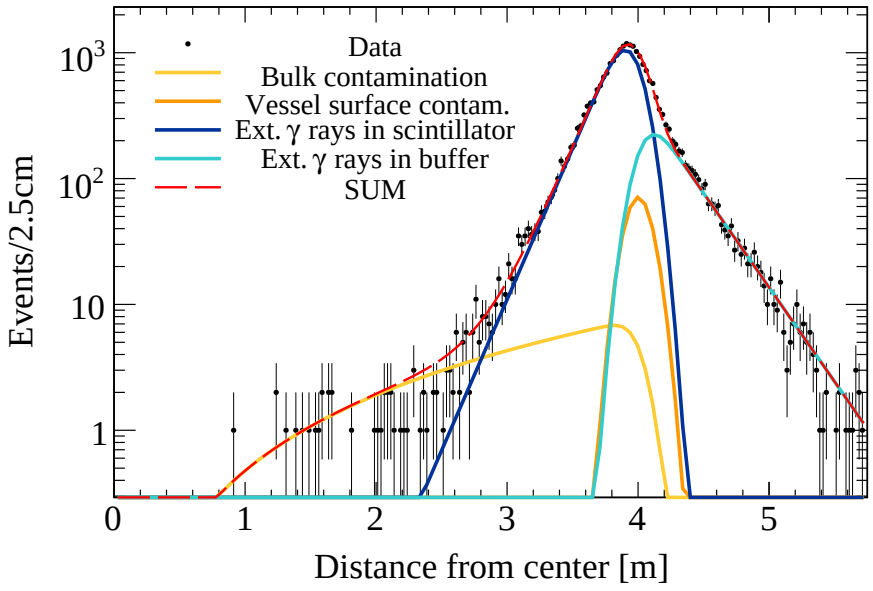

Figure 25. Radial distribution of γ rays induced by the ^{228}Th source placed at 6.85 m distance from the center of detector. The fit includes four components convoluted with the detector response. More details are given in the text.

As it turns out, this attenuation behavior can be well described by an exponential function. Finally, the weighted sum of all four components is convoluted with a Gaussian detector response function. The fit procedure allows to extract several parameters such as the radius of the Inner Vessel. An application of it has already been shown in section 5.3. Moreover, the position resolution and the attenuation length for 2.615 MeV γ rays in PC are determined to be $\sim$11 cm and $\sim$25 cm, respectively. The position resolution is in agreement with the one obtained from the *internal calibration* data (see section 5.2). The attenuation length is in agreement with the reference values provided by the National Institute of Standards and Technology (NIST) database [24].

5.5.3 Total thorium activity in the outer detector components

Materials used for the construction of Borexino were screened prior to installation by means of highly sensitive detection techniques in order to verify their level of radiopurity. For practical reasons, only subsamples of larger batches were screened. For example, this was the case for the stainless steel of the SSS, for the PMTs and the LCs [25]. The estimation of the total radioactivity in the final detector assembly is based on the assumption that the subsamples are representative for the whole batches.

The measurement performed with the ^{228}Th source allows us to measure directly the total activity of thorium A_t in the outer detector components for the first time. This independent measurement can be compared with the overall estimation obtained from the material screening results. The method is based on a comparison of count rates in normal data and in *external calibration* data. For a spherical fiducial volume (FV) with a radial cut at $R<3.0$ m the external background rate in normal data is estimated by a spectral fit, using the shape derived experimentally from *exter-*

2012 JINST 7 P10018

Table 2. Detector components contributing to the external background outside the *Inner Vessel*. The mass fractions of ^{232}Th, ^{238}U and ^{40}K, the total mass of the component and its average distance from the center of detector is included [25–27].

Detector component	^{232}Th [g/g]	^{238}U [g/g]	^{40}K$_{nat}$ [g/g]	Distance from center [cm]	Mass [kg]
SSS	3×10^{-9}	7×10^{-10}	7×10^{-8}	6.85	7×10^{4}
PMT	3.3×10^{-8}	6.6×10^{-8}	2×10^{-5}	6.55	2×10^{3}
Light concentrators	1.8×10^{-7}	1×10^{-9}	1×10^{-5}	6.45	1.2×10^{3}
PC buffer	1×10^{-15}	1×10^{-15}	1×10^{-12}	4.25-6.85	1.04×10^{6}
O.V. Steel endcaps	2×10^{-9}	1×10^{-9}	7×10^{-8}	5.75	1.5×10^{1}
I.V.-O.V. Nylon pipe	5×10^{-11}	5×10^{-11}	7×10^{-7}	–	4.2
I.V. Nylon endcaps	5×10^{-11}	5×10^{-11}	7×10^{-7}	4.25	1.2×10^{1}
Hold down ropes	5×10^{-11}	5×10^{-11}	1×10^{-6}	4.25	4.5
Nylon bag	4×10^{-12}	2×10^{-12}	1×10^{-8}	–	3.2×10^{1}

nal calibration data. The rate is found to be (4.4±1.0) events/(day×100 ton) in the energy region [0.2,3.0] MeV. For the same FV conditions and the same energy range, the rate of events induced by the ^{228}Th source is measured to be ∼3600 events/(day×100 ton). Since the radial position of the source and its activity is well known with an uncertainty of ±3 cm and 6%, respectively, it is possible to deduce the overall activity of the external detector components for the assumption that all of them are located at a distance R=6.85 m from the detector center. This is possible by rescaling the rate observed in normal data with respect to the one measured on calibration data. This leads to

$$A_t(^{228}\mathrm{Th}) = (6.1 \pm 1.4)\ \mathrm{kBq} \tag{5.3}$$

This result is compared with the expectation from the material screening. The main contribution to the external background measured in Borexino comes from the SSS, the PMTs and the LCs. Their distances from the detector center are 6.85 m, 6.25-6.65 m and 6.55-6.85 m, respectively. Moreover, secular equilibrium of the ^{232}Th decay chain is assumed. Then, according to table 2 the total ^{228}Th activities of the three aforementioned components were measured to be 0.3 kBq (SSS), 0.1 kBq (PMTs) and 0.3 kBq (LCs), respectively [25–27]. The corresponding equivalent activity assumed to be due to a single component located at a distance 6.85 m from the center of the detector is

$$A_{t,MS}(^{228}\mathrm{Th}) \sim 4.7\ \mathrm{kBq} \tag{5.4}$$

This value is in good agreement with the result derived from the comparison of Borexino normal and *external calibration* data.

6 Conclusions

The Borexino calibration system has been presented. It includes an internal and an external part, the former used to deploy radioactive sources inside the scintillator, and the latter designed to place γ sources outside of it close to the stainless steel sphere (SSS) and the photomultiplier tubes (PMTs).

2012 JINST 7 P10018

The calibration hardware, sources and procedures were reviewed. Several internal and external calibration campaigns were successfully performed in the period between 2008 and 2011. In total, twelve different α, β, and γ sources were deployed in 295 positions in the highly radio-pure Borexino scintillator without introducing any detectable contamination. Moreover, a 5 MBq ^{228}Th γ source was placed in ten positions close to the surface of the SSS in order to study the external γ ray background originating from the outer detector components.

Several important results were achieved. The position reconstruction algorithm was calibrated at a precision of a few percent using the internal calibration data. As a result, the systematic uncertainty of the fiducial volume and thus of the solar neutrino rate could be drastically reduced [3]. The internal calibration campaigns also provided important information regarding the energy response of the Borexino detector, opening the possibility for a precise determination of the absolute energy scale. Moreover, they allowed us to study the energy reconstruction uniformity within the standard fiducial volumes, as well as asymmetries in position and energy reconstruction due to, for instance, the non-uniform distribution of operational PMTs. The energy spectra and spatial distributions of reconstructed calibration events were also important to test and validate the Borexino Monte Carlo code [23]. The external calibration campaigns allowed us to study both the spectral and the radial shape of the external background in Borexino. Finally, the external calibration data allowed us to determine detector properties such as the shape of the nylon vessel containing the scintillator as well as the thorium content in the external detector components.

The calibration data had a crucial role in the success of Borexino and will have a strong impact on its future physics results. New calibration campaigns will be carried out at the end of the recently begun second phase of the Borexino experiment. Besides further improvement in the precision of the physics results, the new calibration campaigns will allow a long-term stability study of the detector response and of the scintillator properties over a period of more than five years. This is of major importance for future rare-event physics experiments that will be based on organic liquid scintillators as a detection medium.

Acknowledgments

This work was funded by INFN and MIUR PRIN 2007 (Italy), NSF (U.S.A.), BMBF, DFG, and MPG (Germany), NRC Kurchatov Institute (Russia), and MNiSW (Poland). We gratefully acknowledge the generous support of the Laboratori Nazionali del Gran Sasso. We thank the Swiss Paul Scherrer Institut in Villigen, the German Institut für Kernchemie at Johannes-Gutenberg University in Mainz and the German Physikalisch-Technische Bundesanstalt in Braunschweig for their scientific cooperation in the construction and characterisation of the custom-made ^{228}Th source.

References

[1] BOREXINO collaboration, C. Arpesella et al., *First real time detection of ^{7}Be solar neutrinos by Borexino*, *Phys. Lett.* **B 658** (2008) 101 [arXiv:0708.2251].

[2] BOREXINO collaboration, C. Arpesella et al., *Direct Measurement of the ^{7}Be Solar Neutrino Flux with 192 Days of Borexino Data*, *Phys. Rev. Lett.* **101** (2008) 091302 [arXiv:0805.3843].

2012 JINST 7 P10018

[3] THE BOREXINO collaboration, G. Bellini et al., *Precision measurement of the ^{7}Be solar neutrino interaction rate in Borexino*, *Phys. Rev. Lett.* **107** (2011) 141302 [arXiv:1104.1816].

[4] BOREXINO collaboration, G. Bellini et al., *Absence of day-night asymmetry of 862 keV ^{7}Be solar neutrino rate in Borexino and MSW oscillation parameters*, *Phys. Lett.* **B 707** (2012) 22 [arXiv:1104.2150].

[5] BOREXINO collaboration, G. Bellini et al., *Measurement of the solar ^{8}B neutrino rate with a liquid scintillator target and 3 MeV energy threshold in the Borexino detector*, *Phys. Rev.* **D 82** (2010) 033006 [arXiv:0808.2868].

[6] BOREXINO collaboration, G. Bellini et al., *First evidence of pep solar neutrinos by direct detection in Borexino*, *Phys. Rev. Lett.* **108** (2012) 051302 [arXiv:1110.3230].

[7] BOREXINO collaboration, G. Bellini et al., *Observation of Geo-Neutrinos*, *Phys. Lett.* **B 687** (2010) 299 [arXiv:1003.0284].

[8] BOREXINO collaboration, G. Bellini et al., *Study of solar and other unknown anti-neutrino fluxes with Borexino at LNGS*, *Phys. Lett.* **B 696** (2011) 191 [arXiv:1010.0029].

[9] BOREXINO collaboration, G. Bellini et al., *New experimental limits on the Pauli forbidden transitions in ^{12}C nuclei obtained with 485 days Borexino data*, *Phys. Rev.* **C 81** (2010) 034317 [arXiv:0911.0548].

[10] BOREXINO collaboration, G. Bellini et al., *Search for Solar Axions Produced in $p(d,{}^{3}\mathrm{He})\mathrm{A}$ Reaction with Borexino Detector*, *Phys. Rev.* **D 85** (2012) 092003 [arXiv:1203.6258].

[11] BOREXINO collaboration, G. Alimonti et al., *The liquid handling systems for the Borexino solar neutrino detector*, *Nucl. Instrum. Meth.* **A 609** (2009) 58.

[12] BOREXINO collaboration, G. Alimonti et al., *The Borexino detector at the Laboratori Nazionali del Gran Sasso*, *Nucl. Instrum. Meth.* **A 600** (2009) 568 [arXiv:0806.2400].

[13] U.S. Government, Military standard 1246c.

[14] H.O. Back, *Internal radioactive source calibration of the Borexino solar neutrino detector*, Ph.D. thesis, Virginia Polytechnic Institute and State University (2004).

[15] B. Bajcsy et al., *A unified procedure for calibrating intrinsic parameters of spherical lenses*, in *In Vision Interface* **VI 99** (1999) 272.

[16] BOREXINO collaboration, G. Bellini et al., *Muon and Cosmogenic Neutron Detection in Borexino*, 2011 *JINST* **6** P05005 [arXiv:1101.3101].

[17] B. Caccianiga et al., *A multiplexed optical-fiber system for the PMT calibration of the Borexino experiment*, *Nucl. Instrum. Meth.* **A 496** (2003) 353.

[18] S. Hardy, *Measuring the ^{7}Be neutrino flux from the sun: calibration of the Borexino solar neutrino detector*, Ph.D. thesis, Virginia Polytechnic Institute and State University (2010).

[19] W. Maneschg, L. Baudis, R. Dressler, K. Eberhardt, R. Eichler, et al., *Production and characterization of a custom-made ^{228}Th source with reduced neutron source strength for the Borexino experiment*, *Nucl. Instrum. Meth.* **A 680** (2012) 161 [arXiv:1110.1217].

[20] W. Maneschg, *Low-energy solar neutrino spectroscopy with Borexino: Towards the detection of the solar pep and CNO neutrino flux*, Ph.D. thesis, University of Heidelberg (2011).

[21] B. Dasgupta and J. Beacom, *Reconstruction of supernova ν_μ, ν_τ, anti-ν_μ and anti-ν_τ neutrino spectra at scintillator detectors*, *Phys. Rev.* **D 83** (2011) 113006 [arXiv:1103.2768].

2012 JINST 7 P10018

[22] J.B. Birks, *Photophysics of Aromatic Molecules*, *Wiley-Interscience* (1970).

[23] G. Bellini et al., *The Borexino detector response and its full simulation*, in preparation.

[24] M.J. Berger et al., *XCOM: photon cross sections database*, http://www.nist.gov/pml/data/xcom/index.cfm.

[25] BOREXINO collaboration, C. Arpesella et al., *Measurements of extremely low radioactivity levels in Borexino*, *Astropart. Phys.* **18** (2002) 1 [hep-ex/0109031].

[26] L. Cadonati, *The Borexino Solar Neutrino Experiment and its Scintillator Containment Vessel*, Ph.D. thesis, Princeton University (2001).

[27] L. Oberauer, C. Grieb, F. von Feilitzsch and I. Manno, *Light concentrators for Borexino and CTF*, *Nucl. Instrum. Meth.* **A 530** (2004) 453 [physics/0310076].

2012 JINST 7 P10018